

THE PENNSYLVANIA STATE UNIVERSITY
SCHREYER HONORS COLLEGE

DEPARTMENT OF CHEMISTRY

DETERMINATION OF THE SOLUBILITY OF CALCIUM PHOSPHOSILICATE
NANOPARTICLES FOR TARGETED DRUG DELIVERY

JARED M. MAY
SPRING 2019

A thesis
submitted in partial fulfillment
of the requirements
for a baccalaureate degree
in Chemistry
with honors in Chemistry

Reviewed and approved* by the following:

James H. Adair
Professor of Materials Science and Engineering,
Biomedical Engineering, and Pharmacology
Thesis Supervisor

Raymond L. Funk
Professor of Chemistry
Honors Adviser

Raymond E. Schaak
DuPont Professor of Materials Chemistry
Faculty Reader

* Signatures are on file in the Schreyer Honors College.

ABSTRACT

Despite significant advances in treatment options for all types of cancer in recent decades, cancer is still the second leading cause of death in the world. Conventional chemotherapy requires the use of large doses of highly toxic compounds, which leads to systemic side effects due to non-specific cellular uptake, affecting cancer cells and healthy cells alike. Because of this, nanomedicine and targeted strategies have emerged as promising candidates for the new age of cancer treatment. Among current research efforts, calcium phosphosilicate nanoparticles (CPSNPs) are some of the most promising. In the pH 7.4 plasma, CPSNPs are insoluble. Upon reaching the low pH environment of the late endo-lysosome of a cancer cell, the amorphous nanoparticles readily dissolve and release the encapsulated chemotherapeutic agent. CPSNPs can be surface bioconjugated with a wide variety of aptamers to target specific cells and cancers and have shown the ability to encapsulate an extensive array of chemotherapeutics and imaging agents. These nanoparticles have been extensively evaluated in murine models and have shown success in knocking down metastatic tumors, but little is known of their quantitative solubility.

In this study, the chemical solubility of calcium phosphosilicate nanoparticles is investigated to determine a provisional solubility product for the novel material. Calcium ion selective electrodes and inductively coupled plasma – atomic emission spectroscopy are used in conjunction with the electrolyte thermodynamic simulation program from OLI Systems to develop a quantitative solubility of CPSNPs. The solubility of the new material is then examined in simulated physiological conditions. Quantitative knowledge of the solubility of CPSNPs will allow further tailoring of the synthesis to design a nanoparticle that dissolves in highly specific physiological environments to treat a variety of cancers on-demand.

TABLE OF CONTENTS

LIST OF FIGURES	iv
LIST OF TABLES	vii
ACKNOWLEDGEMENTS	ix
Chapter 1 Introduction to Calcium Phosphosilicate Nanoparticles	1
1.1 Background on Nanoparticles for Drug Delivery	1
1.2 Advantages of CPSNPs	4
1.3 Significance of Solubility of CPSNPs	7
Chapter 2 Synthesis and Laundering of Ghost Calcium Phosphosilicate Nanoparticles	11
2.1 Methods and Materials	11
2.1.1 Materials	11
2.1.2 Synthesis of Ghost and Dye Encapsulating CPSNPs	12
2.1.3 Laundering of Calcium Phosphosilicate Nanoparticles	13
2.2 Basic Characterization of CPSNPs	14
2.2.1 Zeta Potential	14
2.2.2 Dye Encapsulation Efficiency using UV-Vis Spectroscopy	17
2.3 Drying and Resuspension of CPSNPs in PBS	18
Chapter 3 Determination of Calcium Activity Using Ion Selective Electrode	19
3.1 Background on Ion Selective Electrodes	19
3.2 Calibration of ISE and Measurement of Calcium Activity	21
3.3 Calcium Ion Activity Results of CPSNPs and Discussion	23
Chapter 4 Stoichiometry of Calcium Phosphosilicate Nanoparticles Using Inductively Coupled Plasma - Atomic Emission Spectroscopy	29
4.1 Introduction to ICP-AES	29
4.2 ICP-AES Methods	31
4.3 ICP-AES Results: Stoichiometry of CPSNPs	32
4.4 Extracting Particle Number Concentrations and Solids Yield from ICP-AES	37
Chapter 5 Integration of Experimental Data into OLI Systems to Determine a Solubility Product for CPSNPs	40
5.1 Introduction to OLI Systems and Electrolyte Thermodynamics Simulations	41
5.2 OLI Systems Parameters for the Solubility of CPSNPs	42
5.3 Experimentally Determined Solubility of CPSNPs	43
5.4 Thermodynamic Analysis of CPSNP Solubility in OLI Systems	44

Appendix A Development of Calcium Ion Selective Electrode Protocol.....	52
Appendix B Development of CPSNP Drying Protocol: The Hydroxyapatite Story ..	54
Appendix C Supplemental Figures and Information	57
BIBLIOGRAPHY.....	60

LIST OF FIGURES

- Figure 1. Solubility curves of select calcium phosphates were generated by OLI Systems using the aqueous database at 25.0 °C. The Log concentrations of aqueous calcium species, including complex ions, were plotted against pH. All calculations were performed with equimolar amounts of solid with respect to calcium and titrated with HCl and NaOH. The red line represents the physiological pH 7.4 where all calcium phosphates are sparingly soluble. In this calculation, a concentration of total calcium equal to 0.1 M was used giving the plateau of solubility at low solution pH.9
- Figure 2. Schematic for the reverse micelle synthesis of calcium phosphosilicate nanoparticles. (A) 29 vol% Igepal® CO-520 in cyclohexane prior to addition of inorganic precursors. (B) Two separate microemulsions form upon addition of aqueous calcium chloride to microemulsion A and aqueous sodium hydrogen phosphate, sodium metasilicate, and the encapsulate RhWT (not pictured) to microemulsion B. (C) Upon combining the two microemulsions, the micelles exchange components and particle growth begins. (D) Agglomeration-growth of CPSNPs is a time dependent process and continues until the particle surfaces are chelated with aqueous citrate. (E) Addition of pH 7.4 ethanol disrupts the micelles and leaves a suspension of CPSNPs. Reprinted from reference 3. 13
- Figure 3. Mean zeta potential and 95% confidence interval of three samples of cit-Ghost-CPSNPs in pH 7.4 70:30 ethanol:water. The samples were measured using the Phase Analysis Light Scattering (PALS) program on a Brookhaven Instruments NanoBrook Analyzer. 15
- Figure 4. Mean particle diameter and 95% confidence interval of three samples of cit-Ghost-CPSNPs in pH 7.4 70:30 ethanol:water. The samples were measured using the dynamic light scattering (DLS) program on a Brookhaven Instruments NanoBrook Analyzer. 16
- Figure 5. Sample calcium ion selective electrode calibration curve corresponding to the measurements in Table 3. A large slope such as the one in the figure is indicative of good electrode performance and allows for precise determination of calcium activities.22
- Figure 6. Calcium ion activity of cit-Ghost-CPSNP samples binned by synthetic batch. Mean Ca^{2+} activities for each synthesis are shown at the base of the corresponding bin and error bars indicate the 95% confidence interval of the results.....25
- Figure 7. Calcium ion activity of cit-Ghost-CPSNP samples binned by tenth of a pH unit observed. Mean calcium activity values for each pH are indicated above the bin and error bars indicate the 95% confidence interval.....26
- Figure 8. Comparison of measured calcium activities of CPSNP samples in 1 volume % PBS solution compared to the calcium activity of hydroxyapatite in the same phosphate-buffered solution. Hydroxyapatite solubility was calculated using OLI Systems and the Aqueous (H^+) framework.28
- Figure 9. Comparison of different elemental ratios presented in CPSNP formulations. The molar ratios of Ca:P:Si seem to cluster to at least four distinct incorporation patterns. This indicates that there is some intrinsic property to the calcium phosphosilicate system that dictates formation of many different phases of varying elemental ratios.....34

- Figure 10. Sample OLI Systems stream input parameters for generic pH 8.7 CPSNPs. The $[\text{Ca}^{2+}]$, $[\text{PO}_4^{3-}]$, $[\text{HPO}_4^{2-}]$, $[\text{H}_2\text{PO}_4^-]$, $[\text{SiO}_2]$, and $[\text{OH}^-]$ obtained from the speciation results were used to develop a provisional k_{sp} for each sample of CPSNPs.....43
- Figure 11. Comparison of the solubility of the calcium phosphosilicate species JMM245 and monocalcium phosphate monohydrate ($\text{Ca}(\text{H}_2\text{PO}_4)_2 \cdot \text{H}_2\text{O}$) using equimolar amounts. Total Aq. (Ca^{2+}) is the sum of all aqueous calcium species and is a more representative proxy of solubility than the concentration of calcium in solution, $[\text{Ca}^{2+}]$, because it accounts for intermediate species. The solubility of JMM245 closely mirrors the solubility of monocalcium phosphate monohydrate, confirming the hypothesis that JMM245 is a monocalcium phosphate-like species.46
- Figure 12. Comparison of the solubility of the calcium phosphosilicate species JMM263 and octacalcium phosphate pentahydrate ($\text{Ca}_8(\text{HPO}_4)_2(\text{PO}_4)_4 \cdot 5\text{H}_2\text{O}$) using equimolar amounts. Total Aq. (Ca^{2+}) is the sum of all aqueous calcium species and is a more representative proxy of solubility than the concentration of calcium in solution, $[\text{Ca}^{2+}]$, because it accounts for intermediate species. The solubility of JMM263 agrees well with the solubility of octacalcium phosphate pentahydrate, again confirming the hypothesis that JMM263 behaves as an octacalcium phosphate-like species.47
- Figure 13. Comparison of the solubility of the calcium phosphosilicate species JMM264 and dicalcium phosphate dihydrate ($\text{CaHPO}_4 \cdot 2\text{H}_2\text{O}$) using equimolar amounts. Total Aq. (Ca^{2+}) is the sum of all aqueous calcium species and is a more representative proxy of solubility than the concentration of calcium in solution, $[\text{Ca}^{2+}]$, because it accounts for intermediate species. The solubility of JMM264 matches well with the solubility of dicalcium phosphate dihydrate, confirming the hypothesis that JMM264 behaves as a dicalcium phosphate-like species.48
- Figure 14. Solubility of calcium phosphosilicate species JMM245, JMM263, and JMM 264 in physiological conditions of human plasma. Human plasma has the composition Na^+ 142, K^+ 5, Mg^{2+} 1.5, Ca^{2+} 2.5, HPO_4^{2-} 1, Cl^- 103, HCO_3^- 27, and SO_4^{2-} 0.5 mmol/L. At pH 7.4 plasma conditions, all calcium phosphosilicate species are insoluble. Upon reaching the pH 5 environment of the late endosome within a cell, the CPSNPs are completely dissolved, thus effectively releasing the encapsulated molecule.50
- Figure 15. Comparison of theoretical calcium activity of hydroxyapatite with experimental calcium activities of Ghost-CPSNP and hydroxyapatite samples, all in 1% PBS. The similarities in activities of cit-Ghost-CPSNP samples and hydroxyapatite samples prompted the hypothesis that recrystallization was occurring during the drying procedure, resulting in hydroxyapatite-coated particles and hydroxyapatite-like results. This hypothesis prompted the development of the current drying protocol, which involves the addition of PBS before drying to prevent dissolution.....55
- Figure 16. Typical formulation sheet for synthetic parameters, chemical lot identifiers, relevant volumes, reaction times, and more describing a typical cit-Ghost CPSNP synthesis.57
- Figure 17. UV-Vis calibration curve used to determine the concentration of RhWT in a cit-RhWT CPSNP sample as a proxy for encapsulation efficiency.58

LIST OF TABLES

Table 1. Review of desired characteristics of nanoparticle delivery systems. Table adapted from references 2 and 5.....	2
Table 2. Brief review of available nanoparticle drug delivery systems. Calcium phosphosilicate nanoparticles, the focus of this study, have a variety of advantages over their contemporaries. Adapted from Yih and Al-Fandi and Adair et al. ^{2,5}	3
Table 3. Sample calcium ion selective electrode calibration steps, volumes added, concentrations, and potential measurements. Measurements were performed on a pre-conditioned Cole-Parmer calcium ion selective combination electrode and a Corning Pinnacle 530 Meter. 21	21
Table 4. Aggregate calcium ion activity results from three aliquots from three samples, JMM 2-45, JMM 2-63 and JMM 2-64. Results include measured electrode potential, determined calcium activity from the calibration curve, measured pH and binned pH to the nearest tenth.23	23
Table 5. Single-factor analysis of variance (ANOVA) comparing the mean measured calcium ion activities across the observed pH range. A p-value of 0.274 indicates that at a 95% confidence interval ($\alpha = 0.05$) there is no significant difference between the mean calcium activities.	27
Table 6: Detection limits of calcium, phosphorus and silicon, the active components of calcium phosphosilicate nanoparticles, in parts per billion (ppb).....	31
Table 7. As received ICP-AES results for three aliquots each from three synthetic batches of 1X cit-Ghost-CPSNPs. Elemental amounts of calcium, phosphorus, and silicon are presented in $\mu\text{g/mL}$. Reported concentrations reflect concentrations in the original samples and take sample preparation into account. ICP-AES analysis was performed by the Institutes of Energy and the Environment Laboratories at the Pennsylvania State University.....	32
Table 8. Molar ratios and 95% confidence interval of molar ratios of JMM 2-45, 2-63 and 2-64 as determined by ICP-AES. The results indicate discrepancies between synthetic batches. For reference, the synthetic elemental ratios are included.....	33
Table 9. Comparison of various calcium phosphates by Ca:P ratio and solubility. Table was adapted from Chow ²⁴ and Sheikh <i>et al.</i> ²⁵	36
Table 10. Comparison of observed Ca:P ratios. Each CPSNP sample can be approximated by a well-studied calcium phosphate system suggesting the constituent ions incorporate into the CPSNP matrix in a manner which mimics these crystalline species, albeit with the addition of silica for stability.	37
Table 11. Provisional solubility products and charge-balanced chemical formulas for each of the three 1X cit-Ghost CPSNP samples analyzed by ICP-AES and calcium ISE. These chemical formulas and solubility data were input into the OLI Systems ESP 9.6 program to create three new species, JMM245, JMM263 and JMM 264, which allowed for their titration and subsequent chemical analysis in OLI Systems.....	44

- Table 12. Specifications of Phosphate Buffered Saline (PBS) from Corning Cellgro. PBS was used to suppress dissolution in calcium ion activity measurements and the species were input into OLI Systems for relevant calculations.58
- Table 13. Relevant inputs and outputs from OLI Studio's Stream Analyzer used to compile a provisional solubility product for each CPSNP sample. The elemental ratios were obtained from ICP-AES analysis and charge-balanced with Na^+ , the dominant secondary cation in the synthesis or OH^- , the standard charge balancing anion of calcium phosphates. Only the input $[\text{Ca}^{2+}]$ and amount of silicate were varied for each pH and synthesis. The calcium added was determined by calcium ion selective electrode and the silicate added was determined via ICP ratio relative to calcium. For calculations, all solid species were excluded to prevent competing reactions.59

ACKNOWLEDGEMENTS

First and foremost, I would like to thank my parents for providing me with every opportunity in life to succeed. They have taught me to chase my dreams, work hard, and be passionate. Despite not being in the field of science themselves, they always encouraged me to pursue my interests in science and medicine and have been my biggest support system throughout my entire life. I would also like to thank my Uncle Jerry for planting the seed of scientific curiosity in me long before I ever took a chemistry course. From a young age, he taught me about solvents and solutes through model rockets and electricity through circuit kits, among many more lessons. I would not be as curious about the world around me without him.

I would also like to thank Dr. James Adair for the mentorship over the past few years of my undergraduate career. His leadership and guidance allowed me to develop a confidence and independence in my research that has translated into other aspects of my life. As the only student with a “chemistry background” working for him, he has let me tackle a wide variety of projects within the group that have made me a better chemist and scientist.

I would also like to recognize members of the Adair research group for their help over the last few years, especially Dr. Chris Gigliotti, Nicholas Gigliotti, and Bernadette Adair. Their assistance and guidance also helped me grow into the scientist I am today.

Lastly, I would like to thank all my friends that have listened patiently when my experiments have failed and congratulated me when they did not. All the support has been greatly appreciated.

Chapter 1

Introduction to Calcium Phosphosilicate Nanoparticles

1.1 Background on Nanoparticles for Drug Delivery

Conventional chemotherapy involves the systemic dosing of agents that do not differentiate between healthy and malignant cells, leaving patients with a wide variety of side effects and often requiring further treatment to counter the undesired side effects.¹ Traditional cancer drugs are nonspecific and highly toxic, creating the delicate balance of choosing a dose that is effective against cancer but mild enough that treatment is not debilitating.² Additionally, many of the current United States Food and Drug Administration approved cancer treatments are not water soluble, requiring them to be administered in an organic solvent, which is often toxic in and of itself.³ To circumvent the use of organic solvents, nanotechnology and various nanoparticle delivery vehicles have been developed to encapsulate the desired drug and address the two chief concerns of specificity and optimal dosing. Among these technologies are biodegradable polymeric nanoparticles, ceramic nanoparticles, dendrimers, liposomes, polymeric micelles, metallic nanoparticles, and calcium-phosphate based nanoparticles.^{4,5} While there is no consensus on the exact definition of a nanoparticle, the National Science Foundation has regarded them as a material with at least one dimension less than 100 nm. Table 1 displays some of the desired characteristics of nanoparticle drug delivery platforms, adapted from Yih and Al-Fandi and Adair et al.^{2,5} Table 2, adapted from the same sources, compares some of the characteristics, advantages, and limitations of the nanoparticle drug delivery systems currently available.

Table 1. Review of desired characteristics of nanoparticle delivery systems. Table adapted from references 2 and 5.

Desired Characteristic	Justification
Inherently non-toxic materials and degradation products	With applications in human health, materials should be non-toxic, and materials used in processing should be non-toxic or able to be effectively eliminated.
Small size (10-200 nm)	A product of synthetic methods, nanoparticles exist in a distribution of sizes and are thus not uniform in diameter. There is not a size that has proven most effective, though considerable research suggests 20-50 nm may be most efficacious for tumor penetration <i>in vivo</i> . The small size allows penetration of even the smallest vasculature and fenestrated capillaries associated with a tumor.
Effective encapsulation of agent at therapeutic levels	Nanoparticle drug delivery vehicles must be able to effectively encapsulate an agent. Surface decoration of chemotherapeutics on nanoparticles is susceptible to degradation of the drug in physiological conditions and thus encapsulation serves to protect the drug.
Colloidally stable in physiological conditions	Physiologically fluids have a specific pH, ionic strength, temperature, osmotic pressure and presence of macromolecules that can make non-ideal delivery vehicles agglomerate and be susceptible to clearance.
Long circulation times	Nanoparticle delivery systems must be stable in circulation long enough to allow the maximum number of particles to reach tumor sites and deliver their cargo before being degraded.
Specific targeting to desired tissue	Ideal nanoparticle platforms are capable of active targeting through surface bioconjugation. Bioconjugation of a protein associated with a receptor of a specific cancer to the exterior of the nanoparticles results in a highly specific treatment.
Biologically controlled release of encapsulated agent	There must be some biological trigger, such as pH or enzymatic reaction, that allows controlled release of the encapsulate into the desired tissue.
Effective clearance mechanism	Nanoparticles must be readily cleared from the body to prevent bioaccumulation from successive treatments.

Table 2. Brief review of available nanoparticle drug delivery systems. Calcium phosphosilicate nanoparticles, the focus of this study, have a variety of advantages over their contemporaries. Adapted from Yih and Al-Fandi and Adair et al.^{2,5}

Nanoparticle Delivery System	Size (nm)	Therapeutic Agents Carried	Advantages	Limitations
Biodegradable Polymers	10-100	Plasmid DNA, proteins, peptides, low MW organics	Sustained, time-released drug delivery	Fixed functionality after synthesis, degrade in bloodstream
Ceramic	<100	Proteins, DNA, chemotherapeutics, high MW organics	Biologically stable, dispersible in water, easily synthesized	Toxic materials, requires surface decoration, not generally bioresorbable
Metallic	<50	Proteins, DNA, chemotherapeutics	Large surface area for ample surface decoration	Toxic materials, requires surface decoration, not bioresorbable
Polymeric Micelles	<100	Proteins, DNA, chemotherapeutics	Hydrophobic core allows for encapsulation of water-insoluble drugs	Toxic precursors and by-products
Liposomes	20-100	Proteins, DNA, RNA, chemotherapeutics	Increased circulation time, reduced systemic toxicity	Poor colloidal stability without surface PEGylation
Dendrimers	<10	Anti-bacterial and anti-viral agents, DNA, chemotherapeutics, high MW organics	Effective for hydrophobic or hydrophilic drugs	Toxic precursors and by-products
Calcium Phosphosilicate Nanoparticles (CPSNPs)	10-60	Chemotherapeutics, RNA, low and high MW organics, imaging agents	Easily prepared, pH dependent dissolution results in intracellular drug delivery, made of bioresorbable materials	Only encapsulates materials soluble in aqueous or select organic solvents

The judicious choice of selecting nanoparticles for cancer drug delivery stems from their many theoretical advantages over conventional therapy methods including large loading capacity, sustained delivery, and protection of the drug from physiological degradation.⁶ Additionally, their abilities can be fine-tuned by altering the size, shape, and surface bioconjugation to target certain cells more accurately. Because nanoparticles are larger than single molecule treatments, they diffuse more slowly through capillary beds in the body. Compared to healthy tissue, tumors are characterized as having poor lymphatic drainage and perforated vasculature as a result of their rapid growth and proliferation.⁶ Upon intravenous injection, nanoparticles and their cargo remain in circulation for long periods of time due to being too large to be filtered and excreted by the kidneys and too small to be recognized by the reticuloendothelial or hepatic systems. As a result, nanoscale therapies leak preferentially into tumor tissue over healthy tissue due to the leaky vasculature of a tumor. These therapies then remain in the tumor tissue due to poor lymphatic clearance.⁶ This selectivity for tumor tissue is known as the enhanced permeability and retention (EPR) effect. The smallest capillaries have diameters of approximately 150 nm, allowing nanoparticles of smaller diameter to rapidly diffuse throughout the entire circulatory system. Likewise, tumor vasculature often has pores of up to 0.3 μm , allowing ample fissures in the tissues for leakage by nanoparticles.⁶

1.2 Advantages of CPSNPs

As described in Table 2, calcium phosphosilicate nanoparticles offer a variety of advantages over their counterparts stemming from their non-toxicity to the multitude of encapsulants and targets possible. CPSNPs are easily synthesized via a reverse micelle synthesis

and are readily laundered to effectively remove cytotoxic surfactant. The synthetic process occurs at room temperature and requires no extreme pressures or conditions and thus is readily prepared using basic laboratory equipment such as magnetic stir plates and separatory funnels. The synthetic process can also be tailored to the desired quantity and concentration of particles by altering the precursor volumes and concentrations and the collection volume.

Perhaps one of the largest benefits of CPSNPs over other nanoparticle drug delivery systems is their inherent non-toxicity and use of bioresorbable materials. Calcium ions and phosphate species are readily present in human plasma solutions at approximately 2.5 and 1.0 mM, respectively.⁷ Additionally, calcium phosphates are the main inorganic constituent of bone and teeth in the form of hydroxyapatite.⁸ Silicate is also present in physiological solutions at a concentration of approximately 0.5 mM, providing further advantages over other nanoparticle systems that use toxic heavy metals, cadmium, selenium or hydrocarbons in their formulations.⁹ Use of bioresorbable materials means that after pH-triggered release of the encapsulate, not only is the nanoparticle vehicle non-toxic, the constituent calcium ions can be utilized in the bone ossification process, muscle contractions, or cellular signaling pathways and phosphates can be incorporated in nucleotide synthesis or bone ossification.

Another advantageous aspect of CPSNPs are their colloidal stability. Current synthetic methods for CPSNPs yield well-dispersed citrate-capped particles with a negative zeta potential. This is advantageous because nanoparticles with a positively charged surface would interact with negatively-charged phosphate groups on cell membranes and would not remain dispersed long enough to reach the target tissue.¹⁰ For CPSNP formulations for *in vivo* injection, the nanoparticles are either functionalized with methoxy-polyethylene glycol or a target-specific aptamer. Methoxy polyethylene glycol-capped (mPEG) nanoparticles display a neutral surface charge and do not

interact with cell membranes. Particles functionalized with an aptamer have surface charges dependent on the aptamer identity.

Another advantage of CPSNPs is their ability to encapsulate a wide variety of imaging molecules and drugs of various sizes. Over time, the Adair research group has been able to encapsulate in appreciable concentrations the organic dyes cascade blue, 10-(3-sulfopropyl) acridinium betaine, fluorescein, indocyanine green, rhodamine WT, and Cy3 amidite as well as biologically active molecules such as insulin, docetaxel, cisplatin, 7-hydroxy-2-dipropyl-aminotetralin (7-OH-DPAT), methotrexate, hexanoyl-ceramide (Cer₆), decanoyl-ceramide (Cer₁₀), Gemcitabine, and 5-fluoro-2'-deoxyuridine 5'-monophosphate.¹⁰ Compared to surface decoration of the desired drug or molecule, encapsulation into the amorphous matrix offers a more viable route to efficient delivery. Encapsulation protects the cargo molecule from degradation in the bloodstream before the nanoparticles are able to reach their target tissue.¹⁰ This protection becomes especially important when the goal is to encapsulate an oligonucleotide for genetic incorporation.

With the encapsulate on the interior of the calcium phosphosilicate nanoparticles, the exterior surface is free to be functionalized with macromolecules to target specific receptors associated with certain cancers, leading to an active targeting of the tumor cells. This active targeting via bioconjugation of macromolecules contrasts with the passive targeting of PEGylated-CPSNPs, which has been shown to prevent protein absorption via formation of a protein corona and maximize retention times in circulation.¹¹ Specifically, CPSNPs have been bioconjugated with human holotransferrin, anti-CD71 antibody, and gastrin peptides. Bioconjugation of human holotransferrin and anti-CD71 antibody target transferrin receptors, which are highly expressed on breast cancer cells compared to healthy tissue.¹¹ Bioconjugation of gastrin peptides targets gastrin

receptors, which are highly expressed on pancreatic cancer tumors.¹¹ By encapsulating the near-infrared imaging agent indocyanine green into the CPSNP matrix, Barth *et al.* showed nanoparticle targeting to the transplanted tumors in mice by capturing a near-infrared image 96 hours after intravenous injection.¹¹ This active targeting decreases the amount of nanoparticles that deliver their cargo incorrectly to healthy tissue and results in an even smaller effective dose needed to treat a cancer, further proving the worth of the CPSNP drug delivery system over bulk drug treatments and other nanoparticle alternatives.

The final desirable characteristic of calcium phosphosilicate nanoparticles is the ease of clearance from the body for nanoparticles that fail to reach their target tissue. Though capable of targeting certain cancers with surface bioconjugation, there are still many receptors and cancers for which we have no aptamer or macromolecule to target. In these scenarios, treatment should be approached using PEGylated-CPSNPs. *In vivo* studies in mice have shown that significant quantities of PEGylated-CPSNPs accumulated in tumors via the EPR effect described above within 24 hours post-injection and particles failing to reach a tumor target were cleared via the hepatobiliary system.¹⁰ Once processed in the liver, the PEGylated-CPSNPs were excreted as fecal matter, assuaging fears of bioaccumulation. These reasons make calcium phosphosilicate nanoparticles desired drug delivery vehicles for study and attractive options for continued research and development.

1.3 Significance of Solubility of CPSNPs

Calcium phosphates were initially chosen as a drug delivery vehicle for their pH-dependent solubility and abundance in physiological solutions. Regardless of calcium:phosphate ratio and

phase, calcium phosphates are insoluble at pH 7.4 (the pH of physiological fluids) and become increasingly soluble below pH 6.^{10,12} This pH-dependent solubility is advantageous because particles will remain intact in plasma following intravenous injection and remain stable until reaching the endo-lysosome of the target cells with pH 4.6-5.^{10,13} At that point, the particles readily dissolve and release the cargo from inside of the cell via the high osmotic pressure within the endo-lysosome. This leads to rupture of the endo-lysosome and introduction of the active agent into the cytosol, inducing apoptosis. Additionally, the local environment surrounding solid tumors presents a pH approximately 0.2 pH units less than healthy tissue and while this change is not typically great enough to induce total dissolution, the CPSNPs will be marginally more soluble in this region.¹⁴ A comparison of the solubility of select calcium phosphates is available in Figure 1.

Silicate was introduced into the matrix by substituting for phosphate to suppress the crystallization of the amorphous calcium phosphate (ACP) into hydroxyapatite. A study by Eanes *et al.* showed that ACP is transformed to crystalline hydroxyapatite in a solution-mediated process.¹⁵ Because the crystallization of an amorphous material inevitably involves a dissolution process, this transformation would release the encapsulate from the matrix and thus silicate doping was included to suppress crystallization. To further prevent transformation to the thermodynamically stable hydroxyapatite, the metastable CPSNPs are stored in either a pH 7.4 70:30 ethanol:water mixture or a pH 7.4 phosphate buffered saline (PBS), which suppresses dissolution via the common ion effect.

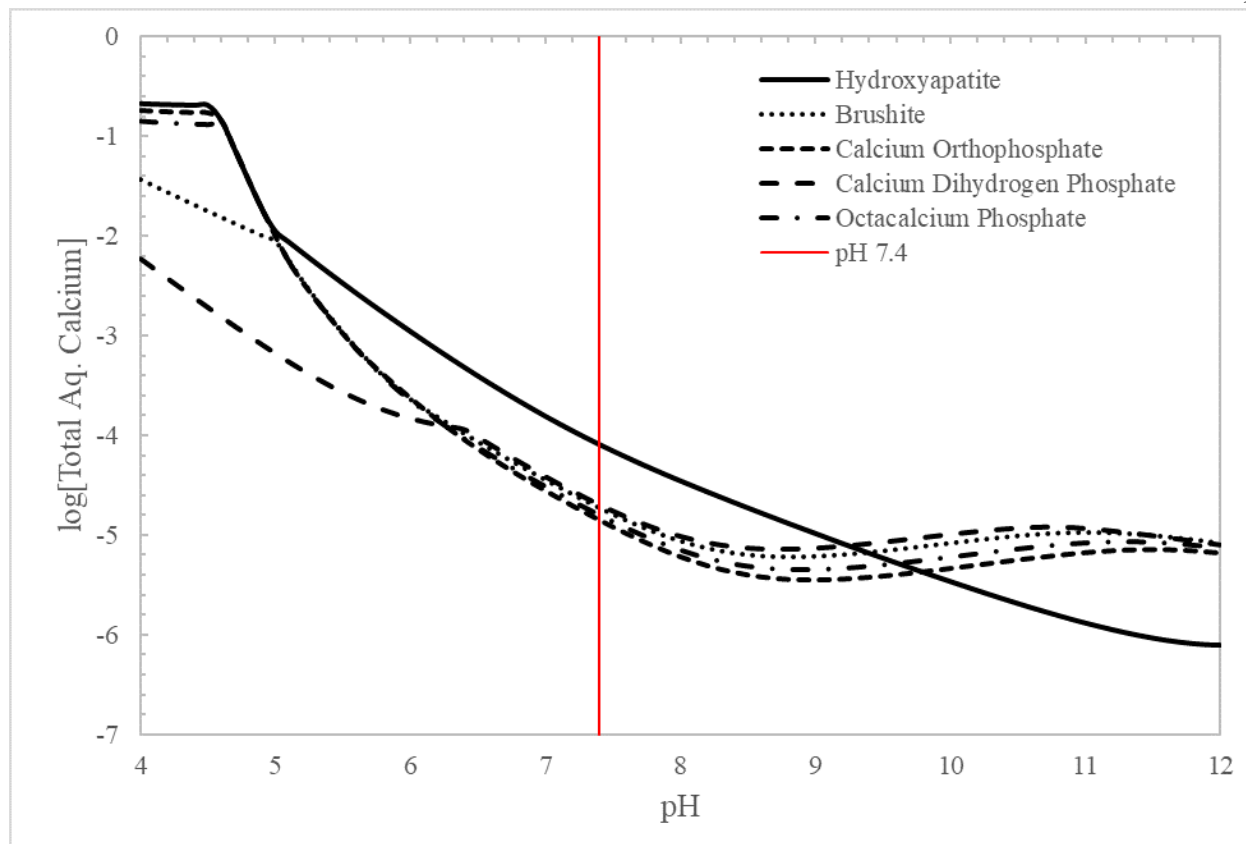


Figure 1. Solubility curves of select calcium phosphates were generated by OLI Systems using the aqueous database at 25.0 °C. The Log concentrations of aqueous calcium species, including complex ions, were plotted against pH. All calculations were performed with equimolar amounts of solid with respect to calcium and titrated with HCl and NaOH. The red line represents the physiological pH 7.4 where all calcium phosphates are sparingly soluble. In this calculation, a concentration of total calcium equal to 0.1 M was used giving the plateau of solubility at low solution pH.

Iterations have determined that the ideal input ratio of Ca:P:Si is 5:3:0.41 and thus is the basis for current formulation inputs. This ratio has similarities to hydroxyapatite, with the molecular formula $\text{Ca}_5(\text{PO}_4)_3\text{OH}$. The dissolution and interfacial properties of hydroxyapatite have been studied extensively by Chander and Fuerstenau,^{8,12} among others, but the pk_{sp} has been seldom agreed upon. Chander and Fuerstenau⁸ present a pk_{sp} of 57.5, Dorozhkin¹⁶ calculated a pk_{sp} of 58.4, Moreno *et al.*¹⁷ determined a pk_{sp} of 58.7, and Clark¹⁸ reported a range of pk_{sp} 's ranging from 57.1 to 58.3. While the exact value is not agreed upon, it is well understood that

hydroxyapatite is thermodynamically stable and sparingly soluble at pH 7.4. As described above, it is understood anecdotally that calcium phosphosilicate nanoparticles exhibit solubility similar to hydroxyapatite and comparable calcium phosphates.¹⁹ The amorphous nature was predicted to increase the solubility at any given pH but was necessary to facilitate efficient encapsulation of the desired drug or imaging agent. The addition of silica into the matrix was predicted to stabilize the particles and decrease solubility and solution-mediated phase transformation. The precise effects of these two opposing forces and the quantitative solubility of the nanoparticles is the basis for this study.

We can characterize the size, morphology and zeta potential of our calcium phosphosilicate nanoparticles. We can determine encapsulation efficiency and cytotoxic surfactant concentration in our formulations. We know precisely how much calcium, phosphate, and silicate is input into the reverse micelle microemulsion synthesis. What we do not know is the exact chemical composition of the product and the stoichiometric ratios. We do not know quantitatively how strongly these ions interact with each other. The goal of this work is to determine a provisional solubility product of the CPSNPs. Knowledge of this value will allow us to fine tune the synthetic parameters by altering the Ca:P:Si ratio to design a composite nanoparticle with a specific solubility to fit a clinical need. This specific control over the solubility of the nanoparticles will allow more efficient targeting of specific pH's associated with various cancers and allow us to better understand our current drug delivery system and design future systems to dissolve selectively at any cancerous site. The goal is to determine experimentally every variable in the below equation.

$$k_{sp} = [\text{Ca}^{2+}]_x [\text{H}_y\text{PO}_4^{3-y}]_z [\text{SiO}_2]_w [\text{OH}^-]_q$$

Chapter 2

Synthesis and Laundering of Ghost Calcium Phosphosilicate Nanoparticles

2.1 Methods and Materials

2.1.1 Materials

The CPSNPs were prepared by the microemulsion technique previously described. Cyclohexane (C_6H_{12} , Sigma-Aldrich), Igepal® CO-520 ($4-(C_9H_{19})C_6H_4(OCH_2CH_2O)_nOH$, Sigma-Aldrich), and deionized H_2O (Millipore Filtration System) were used to prepare the two separate microemulsions. Calcium chloride ($CaCl_2 \cdot 2H_2O$, Sigma-Aldrich), disodium hydrogen phosphate (Na_2HPO_4 , Sigma Aldrich), and sodium metasilicate (Na_2SiO_3 , Sigma-Aldrich) were used as reagent grade precursors to the nanoparticles. Rhodamine WT ($C_{29}H_{29}ClN_2Na_2O_5$, Dyechem) was used as the encapsulate for encapsulation efficiency determination and visualization in the dye-encapsulating particles. Disodium hydrogen citrate dihydrate ($HOC(COOH)(CH_2COONa)_2 \cdot 2H_2O$, Sigma-Aldrich) was used to treat the surface and cease particle growth to the desired size. Neat ethanol was obtained from Pharmco. All deionized water used was purged with Argon (99.998%, Praxair) for at least 20 minutes prior to utilization to remove $CO_2(g)$.

2.1.2 Synthesis of Ghost and Dye Encapsulating CPSNPs

Two separate microemulsions were prepared (A and B). 25.318 g of Igepal® CO-520 and 62.50 mL cyclohexane were added to each microemulsion container and stirred until homogenous at room temperature. Container A received 4.063 mL of 0.1 M $\text{CaCl}_2 \cdot 2\text{H}_2\text{O}$ in degassed water and was stirred for 15 minutes, allowing micelles to form. Container B simultaneously received 0.406 mL of 0.6 M Na_2HPO_4 , 0.406 mL of 0.082 M Na_2SiO_3 , and 3.250 mL of either 0.01 M Rhodamine WT (RhWT, for dye-encapsulating CPSNPs) or degassed-deionized water (for ghost CPSNPs) and was stirred for 15 minutes to facilitate micellular formation. All salts were dissolved in degassed water and all solutions except RhWT were filtered through a cellulose acetate filter prior to addition. After stirring for 15 minutes, the contents of Microemulsion B were added to Microemulsion A and stirred for 2 minutes to undergo micelle exchange. After stirring for 2 minutes, 1.406 mL of 0.1 M disodium citrate was added to the combined microemulsion and stirred for 15 minutes. The microemulsions were then cracked by addition of 313 mL of pH 7.4 ethanol (pH adjusted using KOH) to bring the final synthetic volume to approximately 500 mL. This formulation and replicates will be referred to throughout as 1X cit-Ghost-CPSNPs or 1X cit RhWT-CPSNPs when necessary. A sample synthesis spreadsheet and specifications can be found in Appendix C.

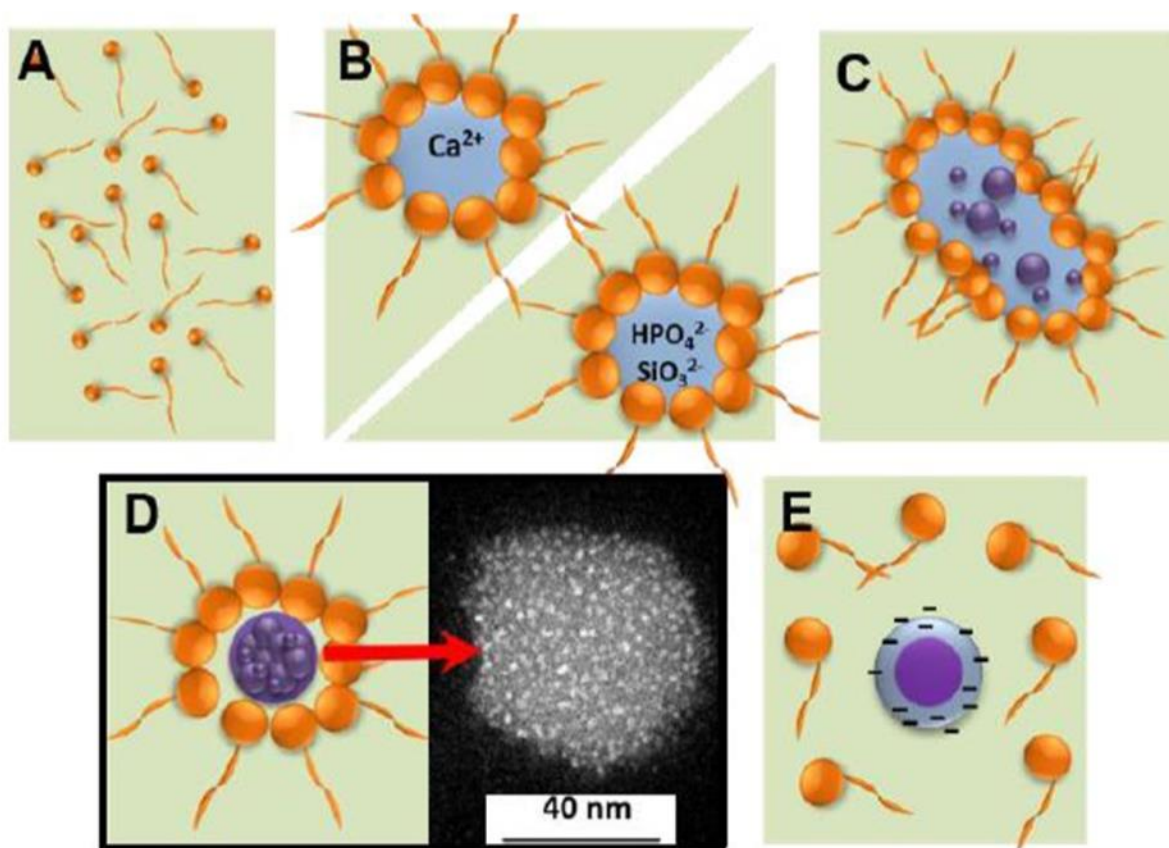


Figure 2. Schematic for the reverse micelle synthesis of calcium phosphosilicate nanoparticles. (A) 29 vol% Igepal® CO-520 in cyclohexane prior to addition of inorganic precursors. (B) Two separate microemulsions form upon addition of aqueous calcium chloride to microemulsion A and aqueous sodium hydrogen phosphate, sodium metasilicate, and the encapsulate RhWT (not pictured) to microemulsion B. (C) Upon combining the two microemulsions, the micelles exchange components and particle growth begins. (D) Agglomeration-growth of CPSNPs is a time dependent process and continues until the particle surfaces are chelated with aqueous citrate. (E) Addition of pH 7.4 ethanol disrupts the micelles and leaves a suspension of CPSNPs. Reprinted from reference 3.

2.1.3 Laundering of Calcium Phosphosilicate Nanoparticles

The nanoparticle suspensions were laundered to remove reagent residues in a proprietary process that is pending technology disclosure. The figures and methods from this section have been omitted. Prior to any further characterization or experimentation, the nanoparticle

suspensions were filtered using 0.22 μm pore regenerative cellulose filters (Corning Inc., Corning, NY) to remove any remaining bacteria or particulates that may have entered solution in processing.

2.2 Basic Characterization of CPSNPs

2.2.1 Zeta Potential

Zeta potential was measured on a Brookhaven Instruments Nano Zeta OMNI Zeta Potential Analyzer (Brookhaven Co., Holtsville, NY). The 1X cit-Ghost-CPSNP suspensions in pH 7.4 70:30 ethanol:water were analyzed and characterized using the phase analysis light scattering (PALS) and dynamic light scattering (DLS) applications at 25.0 °C. The measurement parameters were: viscosity = 2.025 cP, refractive index (η) = 1.363, dielectric constant (ϵ) = 30.23, pH = 7.4. Through 5 measurements for each sample, the mean zeta potential was -22.08 ± 2.03 mV, -34.77 ± 9.97 mV, and -20.36 ± 5.84 mV for JMM 2-45, JMM 2-63, and JMM 2-64, respectively. The results are summarized below in Figure 3.

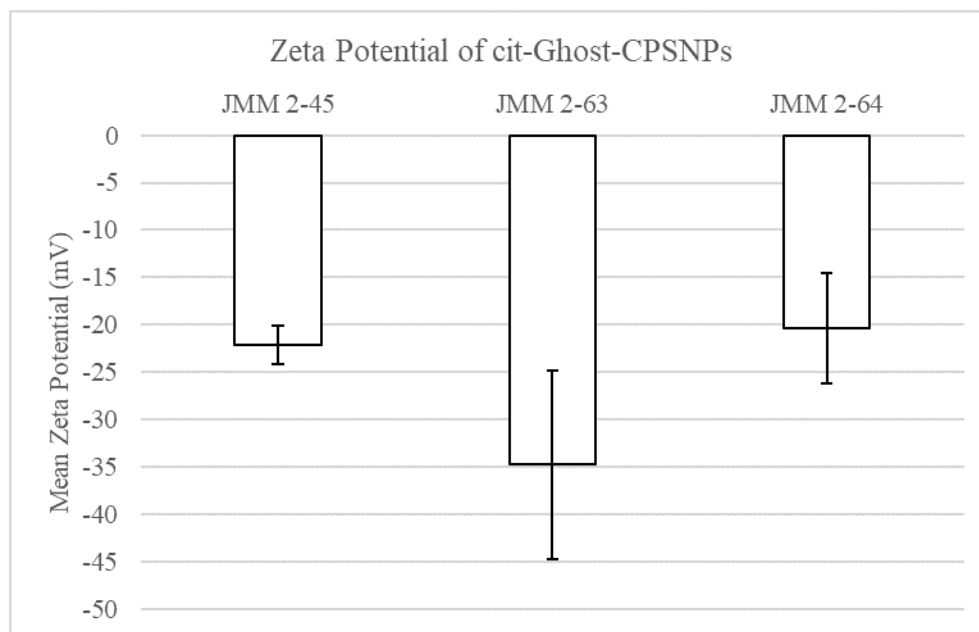


Figure 3. Mean zeta potential and 95% confidence interval of three samples of cit-Ghost-CPSNPs in pH 7.4 70:30 ethanol:water. The samples were measured using the Phase Analysis Light Scattering (PALS) program on a Brookhaven Instruments NanoBrook Analyzer.

The DLS application on the Brookhaven Instruments NanoBrook OMNI Zeta Potential Analyzer was utilized to measure particle size distributions in the same pH 7.4 70:30 ethanol:water suspension. Measurements were performed at pH 7.4 to suppress dissolution of the amorphous calcium phosphosilicate nanoparticles and simulate the physiological conditions of human plasma. Through five measurements for each synthetic batch, the lognormal mean diameters by particle number were 57.76 ± 5.97 nm, 45.20 ± 1.87 nm, and 31.27 ± 11.85 nm for JMM 2-45, JMM 2-63, JMM 2-64 respectively. The DLS and particle size results are summarized below in Figure 4.

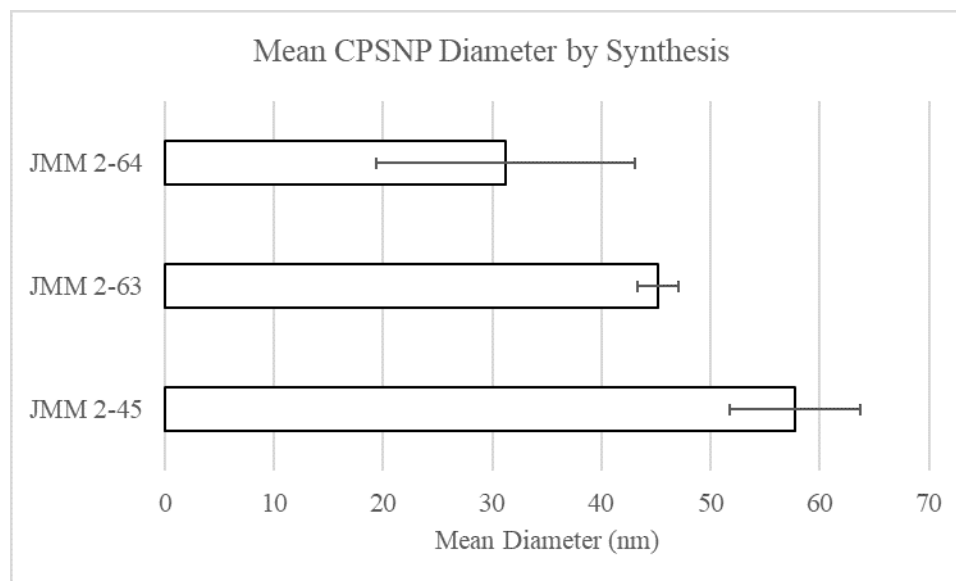


Figure 4. Mean particle diameter and 95% confidence interval of three samples of cit-Ghost-CPSNPs in pH 7.4 70:30 ethanol:water. The samples were measured using the dynamic light scattering (DLS) program on a Brookhaven Instruments NanoBrook Analyzer.

The zeta potential results in Figure 3 above indicate a moderately negatively charged surface and good colloidal stability due to the presence of the negatively charged citrate anion chelated to the surface. Additionally, the range of mean particle diameters from approximately 30-60 nm are suitable for physiological systems. As discussed above, the smallest capillaries have diameters of 150 nm and tumor vasculature has leaky pores of approximately 300 nm in diameter, so these formulations would be ideal.⁶ The discrepancies between syntheses could be due to a variety of factors. The most likely factor causing this is slight variations in reaction times across syntheses. When the calcium microemulsion is combined with the phosphosilicate microemulsion, nucleation and particle growth begin immediately and continue for two minutes until citrate is added to the microemulsion to treat the surfaces and halt agglomeration. Based on the data in Figure 4, it is expected that JMM 2-64 had the least time until surface treatment and JMM 2-45 had the most time until surface treatment. Mere seconds could potentially influence the particle

sizing results. It is also noteworthy that at the time of DLS measurement for particle sizing, JMM 2-45 had been stored for nearly five months while JMM 2-63 and JMM 2-64 had been stored for approximately one month. Though the particles are expected to not agglomerate in the pH 7.4 70:30 ethanol:water mixtures, it is possible some small degree of agglomeration had occurred in that time frame that affected particle size distributions.

2.2.2 Dye Encapsulation Efficiency using UV-Vis Spectroscopy

The calcium phosphosilicate nanoparticles were characterized using UV-Vis spectroscopy to determine concentration of Rhodamine WT (RhWT) dye present in the dye-encapsulating samples relative to the amount used in the synthesis as a measure of encapsulation efficiency. A UV-Star 96 well microplate (Greiner Bio-One, Monroe, NC) and Thermo Labsystems Multiskan Microplate Reader (Rockford, IL) were used to measure the absorbance. As expensive chemotherapeutic drugs are encapsulated in the nanoparticles, it is critical to maximize encapsulate efficiency and not waste material. To measure encapsulate concentration, 50 μL of 1X cit-RhWT-CPSNP suspension was dissolved using 150 μL of 1 mM EDTA solution to chelate the calcium and the absorbance at 548 nm was compared to prepared standards of RhWT and EDTA in pH 7.4 70:30 ethanol:water. Linear analysis yielded a trendline for which the absorbance values for the samples could be used to calculate the concentration of RhWT in the sample, which could be compared to the initial amount of RhWT in the synthesis. This comparison indicated an encapsulation efficiency of $9.07 \pm 0.22\%$. The calibration curve used to calculate the encapsulation efficiency can be found in Appendix C.

2.3 Drying and Resuspension of CPSNPs in PBS

To place the CPSNPs into a suitable medium for characterization of calcium ion activity, treatment of cells, and eventual injections into patients, the 70:30 ethanol:water suspensions were dried and resuspended in a Corning Cellgro phosphate-buffered saline (PBS, 1X without calcium and magnesium, Mediatech, Manassas, VA, specifications and catalog number available in Appendix C) To 10 mL of 1X cit-Ghost-CPSNPs in 70:30, 0.100 mL of PBS (100%) was added, making an approximately 1 volume% PBS in EtOH solution. The sample was then dried under flowing argon to dryness in a 25.0 °C water bath. Once dry, the sample was resuspended with 10 mL of ddH₂O to achieve a 1% volume PBS suspension of CPSNPs for calcium ion activity measurements. The same protocol can be followed to achieve a different desired final concentration of CPSNPs and PBS by altering the volume of sample, PBS added, or resuspension volume.

Chapter 3

Determination of Calcium Activity Using Ion Selective Electrode

3.1 Background on Ion Selective Electrodes

The process of determining a solubility product for the calcium phosphosilicate nanoparticles (CPSNPs) requires a quantitative knowledge of the concentrations and/or activities of individual dissolved ions from the species in solution. Once determined, the product of the concentrations raised to their stoichiometric coefficients in the proposed molecular formula for the particles yields a temperature dependent solubility product for the amorphous material. As the principal cation in the formulation, a calcium ion selective electrode (Ca ISE) was selected as the means to measure the activity of calcium ions in the colloidal nanoparticle solution. It was hypothesized that the large known phosphate concentration of the CPSNPs in a PBS buffer and pH could be combined with the calcium activity measured and elemental analysis to generate all concentrations of ions present besides the silica-species.

To experimentally measure the calcium activity in solution, a Cole-Parmer Calcium Combination Electrode with replaceable membrane, was used to measure the calcium activity in the suspension. Once the ion activity was determined in a buffer of fixed ionic strength, the concentration of calcium in solution can be determined according to the activity coefficients from the Debye-Hückel (1), extended Debye-Hückel (2), and Davies equations (3) in the Ca-P-Si-H₂O system. In the equations below, γ_i is the activity coefficient, I is the ionic strength, z_i is the charge

of a calcium ion, A and B are constants depending on dielectric constant of the solvent, and a_o is the effective diameter of the ion in solution in Å.

$$\log\gamma_i = -Az_i^2\sqrt{I} \quad (1)$$

$$\log\gamma_i = \frac{-Az_i^2\sqrt{I}}{1+Ba_o\sqrt{I}} \quad (2)$$

$$\log\gamma_i = \frac{-Az_i^2\sqrt{I}}{1+\sqrt{I}} + 0.3I \quad (3)$$

Ion selective electrodes function by measuring the potential created by the specific ion against the potential of a reference cell using the Nernst equation (4), where E is the measured potential, R is the universal gas constant, E_0 is the measured potential at a concentration of $C = 1$, T is the temperature, n is the charge of the ion, F is Faraday's constant, C is the concentration of the ion and C_0 is the detection limit. By calibrating using at least two standards that vary in concentration by a factor of 10, a constant slope can be obtained from a graph of the concentration versus potential that can be used to interpolate the concentration of a sample.

$$E = E_0 - 2.303 \frac{RT}{nF} \log(C + C_0) \quad (4)$$

The lower limit of detection for the Cole-Parmer probe is 0.2 ppm or 5×10^{-6} M Ca^{2+} , making the Cole-Parmer probe a suitable instrument for calcium ion analysis given the high stability of the similar hydroxyapatite system. The calcium activities of three samples from each of three CPSNP synthetic batches was determined by calibrating the calcium ISE and measuring the potentials of the CPSNPs suspensions in PBS of fixed ionic strength five times. The reliability of this method was examined by measuring the calcium activity of hydroxyapatite in PBS and comparing the experimental results to theoretical calculations of the solution parameters in OLI Systems at a specific pH. The development and rationale of the calibration method can be found in Appendix A.

3.2 Calibration of ISE and Measurement of Calcium Activity

A calcium ion selective electrode (ISE) with replaceable membrane was obtained from Cole-Parmer and calibrated immediately before each sample measurement. A 10 ppm Ca^{2+} stock solution (20 mL) and 100 ppm Ca^{2+} stock solution (100 mL) were prepared by diluting a 1000 ppm Ca^{2+} standard (Cole-Parmer) with argon-purged deionized water. A 1 vol% PBS solution (100 mL) was prepared by dilution with degassed, deionized water. The reference chamber of the ISE was filled with 4M KCl reference solution (Cole-Parmer) and the internal chamber was filled with the $\text{Ca}^{2+}/\text{Ag}^+$ internal filling solution supplied with the probe. The assembled electrode was carefully swung in a downward motion to remove trapped air bubbles within the apparatus and the membrane was conditioned in 100 mL of 100 ppm Ca^{2+} for 1 hour prior to measurements. The calcium ISE was calibrated by adding specific volumes of 10 ppm Ca^{2+} stock solution stepwise to 100 mL of 1% PBS and measuring the potential on a Corning Pinnacle 530 Meter. The volumes added, resulting concentrations, and example potential measurements are available in Table 3.

Table 3. Sample calcium ion selective electrode calibration steps, volumes added, concentrations, and potential measurements. Measurements were performed on a pre-conditioned Cole-Parmer calcium ion selective combination electrode and a Corning Pinnacle 530 Meter.

Step	Volume of 10 ppm Ca^{2+} Added (mL)	Ca^{2+} (M)	Ca^{2+} (ppm)	1 (mV)	2 (mV)	3 (mV)	Average (mV)
1	0.2	2.00×10^{-6}	0.08	-61	-61	-61	-61
2	0.2	4.00×10^{-6}	0.16	-55	-55	-54	-54.7
3	0.2	6.00×10^{-6}	0.24	-50	-50	-50	-50
4	0.4	9.90×10^{-6}	0.40	-45	-45	-45	-45
5	2.0	2.90×10^{-5}	1.16	-34	-34	-34	-34
6	2.0	4.80×10^{-5}	1.92	-28	-28	-28	-28

The Ca^{2+} concentration in parts per million (ppm) was plotted against the measured potential and fit with a logarithmic curve. Calibration curves with an R^2 value < 0.99 were rejected and repeated. Immediately following calibration, the calcium activity of CPSNP samples was measured at $25.0\text{ }^\circ\text{C}$ in a controlled water bath and determined from the measured potential by the line of best fit. CPSNP samples were dried and resuspended in 1% PBS as described above and equilibrated in an incubator at $25.0\text{ }^\circ\text{C}$ for 24 hours prior to measurement. Each CPSNP sample calcium activity was measured five times and the pH of the sample was measured immediately after, also at $25.0\text{ }^\circ\text{C}$, on an ISFET pH meter. A sample calibration curve is available in Figure 5.

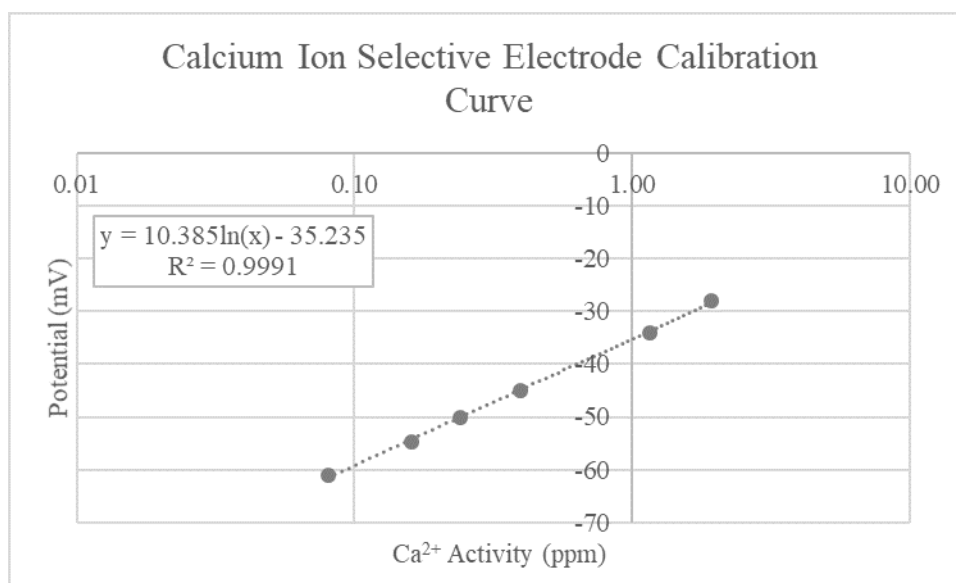


Figure 5. Sample calcium ion selective electrode calibration curve corresponding to the measurements in Table 3. A large slope such as the one in the figure is indicative of good electrode performance and allows for precise determination of calcium activities.

3.3 Calcium Ion Activity Results of CPSNPs and Discussion

Calcium ion activities were measured in three aliquots from three synthetic batches for five measurements each, a total of 45 distinct measurements on 9 total samples. Sample data was then binned by pH and synthetic batch to compare results between aliquots and among syntheses across a narrow pH range. Due to the amorphous nature of the calcium phosphosilicate nanoparticles and inherent error in any measurements, it was expected that the samples would present across a narrow pH range despite the same synthetic procedure, drying protocol, and same measurement protocol for each sample.

Table 4. Aggregate calcium ion activity results from three aliquots from three samples, JMM 2-45, JMM 2-63 and JMM 2-64. Results include measured electrode potential, determined calcium activity from the calibration curve, measured pH and binned pH to the nearest tenth.

Sample	Trial	Temperature (°C)	Measured Potential (mV)	Determined Ca ²⁺ Activity (ppm)	Measured pH	Binned pH
JMM 2-45-1	1	25	70	0.533	8.69	8.7
	2	25	70	0.533	8.69	8.7
	3	25	70	0.533	8.69	8.7
	4	25	71	0.639	8.69	8.7
	5	25	71	0.639	8.69	8.7
JMM 2-45-2	1	25	-32	0.446	8.91	8.9
	2	25	-32	0.446	8.91	8.9
	3	25	-31	0.494	8.91	8.9
	4	25	-31	0.494	8.91	8.9
	5	25	-32	0.446	8.91	8.9
JMM 2-45-3	1	25	-32	0.446	8.90	8.9
	2	25	-31	0.494	8.90	8.9
	3	25	-30	0.547	8.90	8.9
	4	25	-30	0.547	8.90	8.9
	5	25	-32	0.446	8.90	8.9
JMM 2-63-1	1	25	-16	0.432	8.76	8.8
	2	25	-15	0.488	8.76	8.8
	3	25	-15	0.488	8.76	8.8

	4	25	-15	0.488	8.76	8.8
	5	25	-15	0.488	8.76	8.8
JMM 2-63-2	1	25	-24	0.432	8.70	8.7
	2	25	-23	0.486	8.70	8.7
	3	25	-23	0.486	8.70	8.7
	4	25	-24	0.432	8.70	8.7
	5	25	-24	0.432	8.70	8.7
JMM 2-63-3	1	25	-41	0.574	8.84	8.8
	2	25	-42	0.521	8.84	8.8
	3	25	-41	0.574	8.84	8.8
	4	25	-42	0.521	8.84	8.8
	5	25	-42	0.521	8.84	8.8
JMM 2-64-1	1	25	-11	0.502	8.71	8.7
	2	25	-11	0.502	8.71	8.7
	3	25	-11	0.502	8.71	8.7
	4	25	-11	0.502	8.71	8.7
	5	25	-12	0.452	8.71	8.7
JMM 2-64-2	1	25	-23	0.486	8.72	8.7
	2	25	-23	0.486	8.72	8.7
	3	25	-23	0.486	8.72	8.7
	4	25	-23	0.486	8.72	8.7
	5	25	-24	0.432	8.72	8.7
JMM 2-64-3	1	25	-41	0.574	9.04	9.0
	2	25	-42	0.521	9.04	9.0
	3	25	-42	0.521	9.04	9.0
	4	25	-42	0.521	9.04	9.0
	5	25	-42	0.521	9.04	9.0

The simple nature of the calcium phosphosilicate nanoparticle synthesis has resulted in highly reproducible and scalable results in other aspects of characterization. As such, it was expected that the calcium activities would not differ significantly between syntheses despite the amorphous nature of the particles. To compare the results of each synthesis, single-factor analysis of variance (ANOVA) was performed with a 95% confidence interval ($\alpha = 0.05$). The sample JMM 2-45 had an average activity of 0.512 ± 0.063 ppm, JMM 2-63 had an average activity of 0.491 ± 0.045 ppm, and JMM 2-64 had an average activity of 0.500 ± 0.032 ppm. The ANOVA results indicated a p-value of 0.504, indicating there is no significant difference among the three synthetic

batches with a 95% confidence level. The calcium activities of measured 1X cit-Ghost-CPSNP samples binned by synthetic batch are shown below in Figure 6.

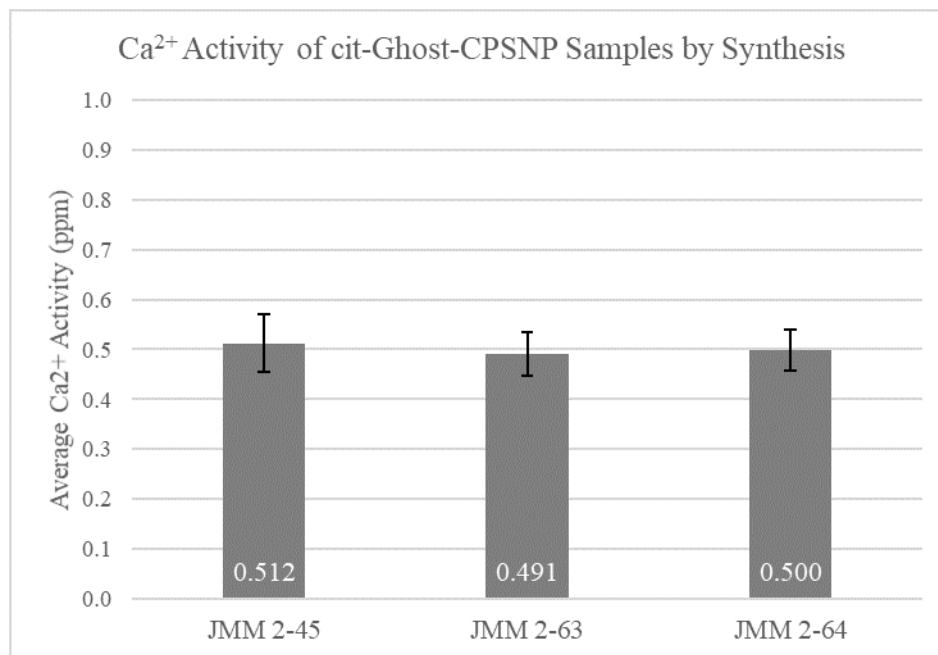


Figure 6. Calcium ion activity of cit-Ghost-CPSNP samples binned by synthetic batch. Mean Ca²⁺ activities for each synthesis are shown at the base of the corresponding bin and error bars indicate the 95% confidence interval of the results.

Similarly, there should be little differences among the samples at each binned pH given the narrow range, identical reaction and measurement conditions, and the small changes in solubility of similar calcium phosphate systems shown in Figure 1. The measured calcium activities, showing little variation between each solution pH bin, are shown in Figure 7. Although Figure 1 suggests that solubility of calcium phosphates increases as pH decreases, evidence of this trend was not observed in the results over the pH range investigated. Partly, this is due to the narrow pH range observed but also may be due to a local or global minimum in solubility over this pH range. Further experimentation across wide pH ranges or integration of the current data with complex

computations in computer programs will be needed to resolve the solubility across a wider pH range.

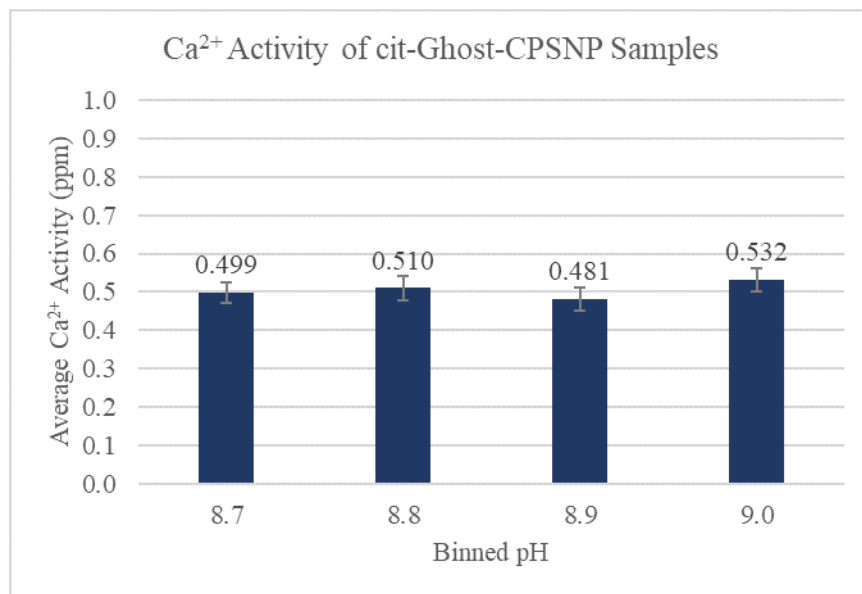


Figure 7. Calcium ion activity of cit-Ghost-CPSNP samples binned by tenth of a pH unit observed. Mean calcium activity values for each pH are indicated above the bin and error bars indicate the 95% confidence interval.

To determine if the slight differences among the mean calcium activities of each binned pH were significant, single-factor analysis of variance (ANOVA) was performed. The results of ANOVA can be found in Table 5. Despite the variation between pH bins, at $\alpha = 0.05$, a p-value of 0.274 indicates that there is no significant difference among the calcium activity results when binned by pH. The results of ANOVA can be found in Table 5, which also highlights the variance of each grouping and number of samples in each group.

Table 5. Single-factor analysis of variance (ANOVA) comparing the mean measured calcium ion activities across the observed pH range. A p-value of 0.274 indicates that at a 95% confidence interval ($\alpha = 0.05$) there is no significant difference between the mean calcium activities.

SUMMARY

<i>Groups</i>	<i>Count</i>	<i>Sum</i>	<i>Average</i>	<i>Variance</i>
8.7	20	9.978	0.499	0.003
8.8	10	5.097	0.510	0.002
8.9	10	4.809	0.481	0.002
9.0	5	2.659	0.532	0.001

ANOVA

<i>Source of Variation</i>	<i>SS</i>	<i>df</i>	<i>MS</i>	<i>F</i>	<i>P-value</i>	<i>F crit</i>
Between Groups	0.010	3	0.003	1.343	0.274	2.833
Within Groups	0.098	41	0.002			
Total	0.108	44				

With statistically valid calcium activity results now developed for cit-Ghost-CPSNPs in 1 volume % PBS across a pH range from 8.7 to 9.0, the results were compared to the theoretical calcium activity of saturated hydroxyapatite in the same 1 volume % PBS conditions using the OLI Systems database. Initial calculations for hydroxyapatite, shown in Figure 8, indicate that the calcium phosphosilicate nanoparticles are significantly more soluble at the pH range observed than hydroxyapatite. These results agree with the hypothesis that amorphous materials will be more soluble than their thermodynamically stable crystalline form. Hydroxyapatite is the thermodynamically stable form of calcium phosphate and was therefore expected to be less soluble than the metastable calcium phosphosilicate nanoparticles. It was also hypothesized that the introduction of silica would aid in stabilizing the matrix to prevent a solution-mediated crystallization into hydroxyapatite based on the experience of the Adair research group.

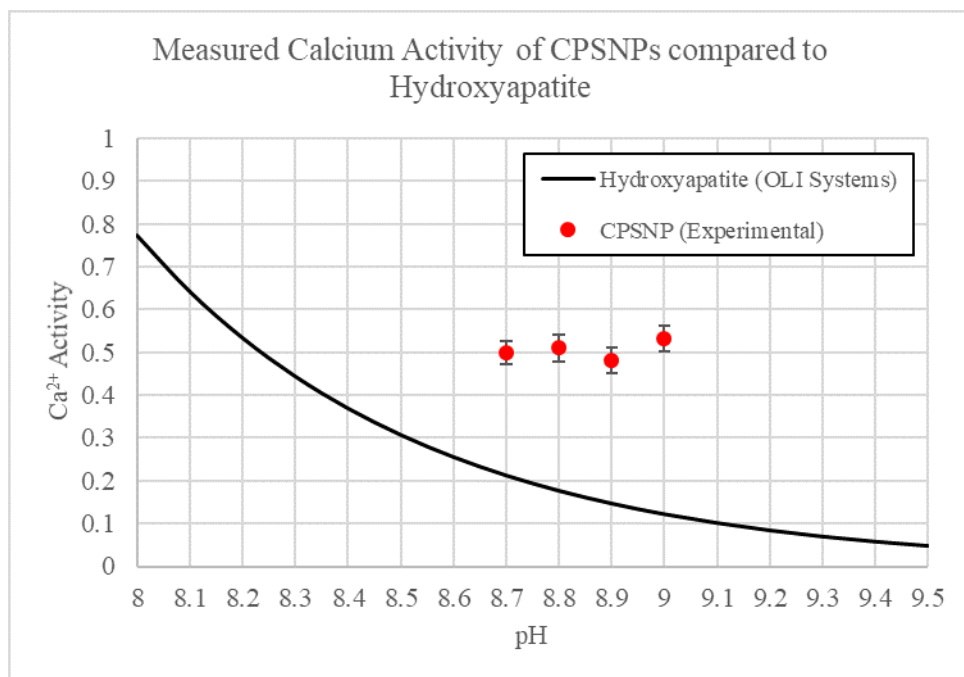


Figure 8. Comparison of measured calcium activities of CPSNP samples in 1 volume % PBS solution compared to the calcium activity of hydroxyapatite in the same phosphate-buffered solution. Hydroxyapatite solubility was calculated using OLI Systems and the Aqueous (H^+) framework.

Chapter 4

Stoichiometry of Calcium Phosphosilicate Nanoparticles Using Inductively Coupled Plasma - Atomic Emission Spectroscopy

As a critical component of the provisional solubility product of a novel material, it was necessary to determine the stoichiometric ratios of each principal element in calcium phosphosilicate nanoparticles in order to understand how the constituent ions are quantitatively incorporated into the amorphous matrix. Although elemental ratios of CPSNPs were previously established by Altinoglu²⁰ using electron energy loss spectroscopy (EELS) during a scanning transmission electron microscopy (STEM) study, slight modifications and improvements to the synthetic procedure over the years and the development of a scaled-up synthetic protocol justified the need for current data on elemental ratios. Altinoglu previously determined atomic percent ratios of 32:55:13 for Ca:P:Si using EELS, which differs significantly from the synthetic input ratios of 59:36:5.²⁰

4.1 Introduction to ICP-AES

Since the introduction in 1974, Inductively Coupled Plasma – Atomic Emission Spectroscopy (ICP-AES) has become the most common choice for multielement analysis by optical spectroscopy due to the low limits of detection and ability to accurately detect over 70 different elements.²¹ Liquid samples are typically nebulized into aerosols and injected into the instrument for analysis, though laser ablation techniques exist for thin film or solid analysis. Once excited by the plasma, each element in the sample emits a characteristic spectrum in the ultraviolet

or visible range. A detector measures this light intensity and the intensity at a particular wavelength is proportional to the concentration of the particular element.

Similar to AES, ICP can be coupled with a mass spectrometer to measure charge to size ratios of ionized components of the sample, which typically produce lower detection limits than AES but may suffer from matrix interferences. Additionally, ICP-MS systems are more expensive and require increased maintenance and operational difficulty.²² For these reasons, ICP-AES was chosen as the primary method to quantitatively determine stoichiometric ratios of elements in CPSNP samples.

The accuracy of ICP-AES is dependent on the element of interest and calibration standards but the measurement accuracy is as low as 0.5%, providing ample applications in geological analysis, trace analysis of metal alloys, analysis of nuclear materials and in semiconductor processing.²¹

ICP-AES instruments consist of three main parts: sample injection system, plasma torch, and optical detector. Initially, liquid samples are introduced as aerosol droplets by a pneumatic nebulizer. The gas flow rate and sample uptake rate are controlled to optimize droplet size, as droplets too large vaporize ineffectively.²³ Optimal droplet size is less than 10 μm in diameter.²¹ The plasma torch is generally argon-based in a quartz tube and is generated using a radio frequency generator at 27 MHz attached to an induction coil surrounding the argon tube.²¹ As a strong magnetic field develops, a seed spark is used to activate the argon gas, producing ions.²² As the current flows in a closed circle, the plasma torch can reach temperatures in excess of 8000 K. In the plasma torch, sample solvent is rapidly evaporated, the sample chemical bonds are destroyed and energy is transferred to sample atoms and ions via collisions.²¹ Only ionized elements produce emissions, so elements with small ionization energies emit more intensely than other elements.²³

The detector measures emissions in the ultraviolet and visible wavelength regions. Emissions are element specific, permitting multiple elements to be analyzed simultaneously by using a polychromator detector.

The biggest source of error in ICP-AES is spectral overlaps between elements of interest. Many elements produce emissions at multiple wavelengths, so secondary wavelengths can be chosen to negate the interference. Spectral interferences can also be subtracted from the emissions if the magnitude is known.²¹ The presence of organic solvents or differences in the concentration of acid used to digest samples can also have an impact on the accuracy of ICP-AES.²¹ For these reasons, samples were dried from their as-synthesized suspensions to remove ethanol and digested in the same concentration of acid as the calibration standards. Detection limits for ICP-AES depend on the element of interest but are typically sub- $\mu\text{g/mL}$. Detection limits for the elements of interest in this study are shown in Table 6.

Table 6: Detection limits of calcium, phosphorus and silicon, the active components of calcium phosphosilicate nanoparticles, in parts per billion (ppb).

Element	Detection Limit (ppb)²¹
Ca	0.1-1.0
P	50-100
Si	10-50

4.2 ICP-AES Methods

Inductively coupled plasma – atomic emission spectroscopy was performed by the Institutes of Energy and the Environment Laboratories at The Pennsylvania State University. Filtered (0.22 μm pore regenerative cellulose filters, Corning Inc., Corning, NY) 1X cit-Ghost-CPSNP samples (4 mL) in pH 7.4 70:30 ethanol:water suspensions were dried down in acid-

cleaned PFA vials at 15.5 °C. After drying to a solid, 2 mL of 4 M HNO₃ was added to the vials and sealed for particle digestion at 43 °C for 16 hours. The samples were then dried again at 43 °C. Once dry, 10 mL of 0.3 M HNO₃ was added and this solution was analyzed and compared to EPA standards for calcium, phosphorus, and silicon. The reported concentrations reflected the concentrations in the original samples and took sample preparation into account.

4.3 ICP-AES Results: Stoichiometry of CPSNPs

The ICP-AES results indicated variable elemental ratios in CPSNP formulations despite identical synthetic protocols. Inconsistent results could stem from a variety of causes that will be explored throughout this section. The variant results confirm the hypothesis that the nanoparticles are an amorphous material: if calcium phosphosilicate were indeed a novel *crystalline* material, the elemental ratios between syntheses would be identical, assuming a thermodynamically stable phase is formed. The unprocessed ICP-AES results are presented in Table 7.

Table 7. As received ICP-AES results for three aliquots each from three synthetic batches of 1X cit-Ghost-CPSNPs. Elemental amounts of calcium, phosphorus, and silicon are presented in µg/mL. Reported concentrations reflect concentrations in the original samples and take sample preparation into account. ICP-AES analysis was performed by the Institutes of Energy and the Environment Laboratories at the Pennsylvania State University.

Element	Ca (µg/mL)	P (µg/mL)	Si (µg/mL)
JMM 2-45-1	1.31	2.57	2.59
JMM 2-45-2	1.17	2.50	2.33
JMM 2-45-3	1.30	2.82	2.68
JMM 2-63-1	4.14	2.41	2.88
JMM 2-63-2	3.68	2.29	2.64
JMM 2-63-3	4.16	2.42	3.17
JMM 2-64-1	3.92	2.77	2.51
JMM 2-64-2	3.70	2.69	2.77
JMM 2-64-3	3.85	2.68	2.50

To compare elemental ratios within and between syntheses, each synthetic batch was averaged and converted to molar ratios for each element. Conversion into molar ratios highlighted the variation between synthetic batches. Molar ratios and the 95% confidence interval (based on the three replicate measurements of each synthesis) are reported below in Table 8. Synthetic parameters are also included for reference. For reference, the elemental ratios for Ca:P:Si used in syntheses are 59.5:35.7:4.9.

Table 8. Molar ratios and 95% confidence interval of molar ratios of JMM 2-45, 2-63 and 2-64 as determined by ICP-AES. The results indicate discrepancies between synthetic batches. For reference, the synthetic elemental ratios are included.

Molar Ratios (%) and 95% Confidence Interval			
<i>Synthetic Batch</i>	<i>Ca</i>	<i>P</i>	<i>Si</i>
JMM 2-45	15.2 ± 1.1	41.1 ± 2.6	43.7 ± 1.7
JMM 2-63	35.7 ± 1.6	27.5 ± 2.4	36.9 ± 3.0
JMM 2-64	34.7 ± 3.0	31.8 ± 1.3	33.5 ± 4.3
Synthetic Parameters	59.5	35.7	4.9

Clearly, discrepancies exist among the synthetic batches and the input elemental ratios. Calcium, phosphate, and silicate are not being incorporated into the CPSNP matrix stoichiometrically in the same ratio as they are combined. Additionally, silicate is being incorporated into the matrix at a higher rate than other ions, considering it is the minor element added in synthesis. The input ratios were engineered to mimic hydroxyapatite so that an amorphous material, with the same Ca:P ratio as hydroxyapatite, could be incorporated into a nanoparticle and doped with silicate (in any phase) to stabilize the metastable species. By normalizing the ratio of ions input to how they are presented in hydroxyapatite, CPSNPs should have theoretical stoichiometric coefficients of 5:3:0.41, assuming 100% incorporation of each ion input. The molar

ratios in Table 8 indicate that the constituent ions are not incorporated in the predicted pseudo-hydroxyapatite manner. The anomalous results prompted comparisons to other elemental ratios in CPSNPs measured previously. The samples JMM 2-17 and JMM 1-22 were previously synthesized 1X cit-Ghost-CPSNP samples and the sample labeled “Altinoglu EELS Data” was from a fluorophore encapsulating cit-CPSNP in his dissertation, obtained via electron energy loss spectroscopy.²⁰

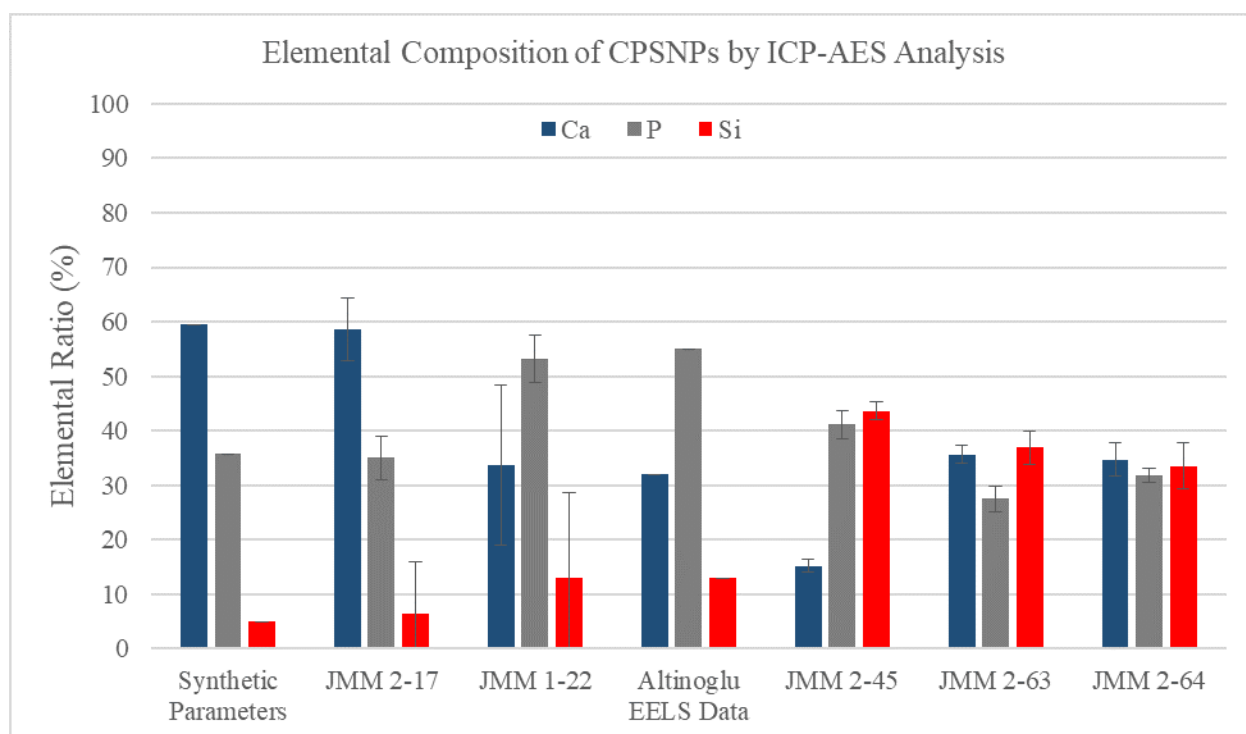


Figure 9. Comparison of different elemental ratios presented in CPSNP formulations. The molar ratios of Ca:P:Si seem to cluster to at least four distinct incorporation patterns. This indicates that there is some intrinsic property to the calcium phosphosilicate system that dictates formation of many different phases of varying elemental ratios.

From the comparison of elemental composition in six cit-CPSNP samples and the synthetic parameters, it is evident that CPSNPs do not form in a uniform amorphous phase, but rather partition into a variety of calcium phosphosilicate phases and ratios. The sample JMM 2-17 partitioned quite well to match the synthetic parameters, matching the molar ratios presented in

the silicate-doped hydroxyapatite hypothesis proposed. The EELS elemental ratios collected by Altinoglu in 2010 agree with the ICP-AES data collected in 2018 on sample JMM 1-22. It is important to note that JMM 1-22 and Altinoglu's sample were synthesized in the small-scale procedure, which was common before the scaled-up procedure was developed, from which all other samples were synthesized. The two recent samples, JMM 2-63 and JMM 2-64, which were synthesized side-by-side on the same day, have relatively close elemental ratios, though the Ca:P ratios differ slightly. Lastly, the molar ratios of JMM 2-45 represented the fourth unique calcium phosphosilicate phase formed and is unlike any other CPSNP species formed in terms of elemental ratios.

The data above in Figure 9 can be rationalized according to a new hypothesis: calcium and phosphate incorporate into the calcium phosphosilicate nanoparticle matrix in similar Ca:P ratios observed in various calcium phosphates and are doped by amounts of silica that vary according to the calcium phosphate. Calcium phosphates with a variety of Ca:P ratios exist and have been well-studied in a variety of Ca:P ratios ranging from 0.5 to 2.0.²⁴ Table 9 presents a summary of calcium phosphates, their chemical formula, solubility, and Ca:P ratios, adapted from two separate reviews on calcium phosphates.^{24,25}

Table 9. Comparison of various calcium phosphates by Ca:P ratio and solubility. Table was adapted from Chow²⁴ and Sheikh *et al.*²⁵

<i>Compound Name</i>	<i>Chemical Formula</i>	<i>Ca:P Ratio</i>	<i>p_{k_{sp}} at 25 °C</i>
Monocalcium phosphate monohydrate	Ca(H ₂ PO ₄) ₂ ·H ₂ O	0.5	Highly soluble
Monocalcium phosphate anhydrous	Ca(H ₂ PO ₄) ₂	0.5	Highly soluble
Dicalcium phosphate dihydrate (Brushite)	CaHPO ₄ ·2H ₂ O	1.0	6.59
Dicalcium phosphate anhydrous (Monetite)	CaHPO ₄	1.0	6.90
Octacalcium phosphate pentahydrate	Ca ₈ (HPO ₄) ₂ (PO ₄) ₄ ·5H ₂ O	1.33	96.6
Precipitated hydroxyapatite	Ca _{10-x} (HPO ₄) _x (PO ₄) _{6-x} (OH) _{2-x} (0 < x < 1)	1.33-1.67	Variable
Calcium-deficient hydroxyapatite	Ca _{10-x} (HPO ₄) _x (PO ₄) _{6-x} (OH) _{2-x} (0 < x < 1)	1.5-1.67	Variable
Hydroxyapatite	Ca ₅ (PO ₄) ₃ OH	1.67	58.4

By comparing the experimental results to well-studied Ca:P ratios in other calcium phosphate systems, each sample analyzed can be directly compared to a known calcium phosphate based on Ca:P ratio. The synthetic parameters and JMM 2-17 present in a hydroxyapatite-like system. Altinoglu's EELS sample, JMM 1-22, and JMM 2-45 can all be approximated to a monocalcium phosphate-like system. The octacalcium phosphate system approximates the sample JMM 2-63 and the sample JMM 2-64 can be approximated by a dicalcium phosphate-like system (brushite). These results suggest that CPSNP synthesis is not a uniform process, and slight changes in timing, temperature, and other variables can affect synthesis and cause the nanoparticles to partition into the calcium phosphate phases below in Table 10 in an amorphous nature stabilized by the addition of silicate. Further studies will be needed to fully understand these effects. It is important to note that the different observed Ca:P ratios had no noticeable effect on particle size, zeta potential, or calcium ion activity.

Table 10. Comparison of observed Ca:P ratios. Each CPSNP sample can be approximated by a well-studied calcium phosphate system suggesting the constituent ions incorporate into the CPSNP matrix in a manner which mimics these crystalline species, albeit with the addition of silica for stability.

<i>Sample/Specifications</i>	<i>Ca:P Ratio</i>	<i>Similar Ca:P System</i>
Synthetic Parameters	1.67	Hydroxyapatite-like
JMM 2-17	1.67	Hydroxyapatite-like
JMM 1-22	0.63	Monocalcium phosphate-like
Altinoglu EELS Data	0.58	Monocalcium phosphate-like
JMM 2-45	0.37	Monocalcium phosphate-like
JMM 2-63	1.30	Octacalcium phosphate-like
JMM 2-64	1.09	Dicalcium phosphate-like

4.4 Extracting Particle Number Concentrations and Solids Yield from ICP-AES

Particle number concentration is a useful metric for evaluating the loading capacity of a nanoparticle suspension, which is relevant to the suspension capacity for encapsulating and delivering chemotherapeutics efficiently. In Altinoglu's dissertation,²⁰ he determined a particle number concentration of $1.9 \times 10^{13} \frac{\text{particles}}{\text{mL}}$, but this number assumed 100% yield, a number that is likely not achievable. To achieve this calculation, stoichiometric ratios from the EELS data were also used. With the new concentrations and updated elemental ratios determined from ICP-AES, a particle number concentration based on experimental results was calculated for each of the three samples analyzed by ICP-AES.

The total mass of calcium phosphosilicate nanoparticles can be calculated using the concentrations of elemental calcium in the ICP-AES results. For the sample JMM 2-45, based on

the chemical formula $\text{CaNa}_{0.7}(\text{H}_2\text{PO}_4)_{2.7}(\text{SiO}_2)_{2.87}$ and an average concentration of Ca in ICP analysis of $31.4 \mu\text{mol/L}$, the mass of CPSNPs is calculated as follows:

$$31.4 \frac{\mu\text{mol}}{\text{L}} \left(\frac{1 \text{ mol Ca}}{1 \text{ mol CPSNP}} \right) \left(\frac{0.5 \text{ L}}{\text{synthesis}} \right) = 15.7 \times 10^{-6} \text{ mol/synthesis}$$

$$15.7 \times 10^{-6} \left(\frac{490.479 \text{ g}}{\text{mol}} \right) = 7.70 \times 10^{-3} \frac{\text{g CPSNP}}{\text{synthesis}}$$

assuming a formula weight of 490.479 g/mol . The mass of an individual calcium phosphosilicate nanoparticle is then calculated as follows:

$$\text{Volume CPSNP} = \frac{4}{3} \pi \left(\frac{d}{2} \right)^3 = 1.01 \times 10^{-16} \frac{\text{mL}}{\text{particle}}$$

$$1.01 \times 10^{-16} \frac{\text{mL}}{\text{particle}} \left(\frac{2.23 \text{ g}}{\text{mL}} \right) = 2.25 \times 10^{-16} \frac{\text{g}}{\text{particle}}$$

where the mean diameter (d) for JMM 2-45 is 58 nm , as determined above. The density used, 2.23 g/mL , is the density of monocalcium phosphate monohydrate,²⁵ the most closely related known calcium phosphate species by Ca:P ratio. The predicted monolayer surface coverage of citrate for each nanoparticle was considered to contribute negligibly to the density and particle diameter. To compute a particle number for a 500 mL standard large-scale synthesis, the mass of CPSNP was divided by the mass per particle as follows:

$$N_{\text{CPSNP}} = \left(\frac{7.70 \times 10^{-3} \text{ g}}{2.25 \times 10^{-16} \frac{\text{g}}{\text{particle}}} \right) = 3.42 \times 10^{13} \frac{\text{particles}}{\text{synthesis}}$$

$$3.42 \times 10^{13} \frac{\text{particles}}{\text{synthesis}} \left(\frac{\text{synthesis}}{500 \text{ mL}} \right) = 6.84 \times 10^{10} \frac{\text{particles}}{\text{mL}}$$

Following these same assumptions and equations, the particle number concentrations for samples JMM 2-63 and JMM 2-64 can also be calculated to be 1.40×10^{11} and 4.91×10^{11} particles/mL, respectively. For the sample JMM 2-63, it assumes a chemical formula of

$\text{Ca}_8\text{Na}_{0.43}(\text{PO}_4)_{4.11}(\text{HPO}_4)_{2.05}(\text{SiO}_2)_{8.27}$, molar mass of 1414.497 g/mol, average particle diameter of 45 nm determined previously for the sample, and density of 2.61 g/mL, the reported density of octacalcium phosphate.²⁵ For sample JMM 2-64, a chemical formula of $\text{Ca}(\text{HPO}_4)_{0.92}(\text{SiO}_2)_{0.97}(\text{OH})_{0.16}$, molar mass of 189.382 g/mol, average particle diameter of 31 nm determined previously for the sample, and density of 2.27 g/mL, the reported density of dicalcium phosphate dehydrate,²⁵ were used. To determine the chemical formula of each species, the Ca:P ratios were compared to the most similar known calcium phosphate species, which served as a model for the protonation state of the CPSNP species. The amount of calcium was normalized to the known species and the relative amounts of associated phosphates and SiO_2 were added. The particle was charge-balanced by the addition of sodium cations or hydroxide anions. Sodium was chosen as the cation for charge balance due to the abundance in the synthetic parameters. Hydroxide was chosen as the anion to mimic the charge-balance of some known calcium phosphates, including hydroxyapatite.

These determined values are significantly less than the previously reported particle number concentration of $1.9 \times 10^{13} \frac{\text{particles}}{\text{mL}}$, but previous calculations assumed 100% yield. By using measured ICP-AES elemental concentrations as a proxy for determining particle number, a more accurate value can be achieved. By comparing the moles of elemental calcium in the ICP-AES results to the amount used in a synthesis (4.06×10^{-4} moles), percent incorporation yields can be calculated for each synthesis. The samples JMM 2-45, JMM 2-63, and JMM 2-64 achieved reaction incorporation yields of 3.9%, 12.3%, and 11.7%, respectively, for calcium ions.

Chapter 5

Integration of Experimental Data into OLI Systems to Determine a Solubility Product for CPSNPs

The OLI Systems, Inc. Stream Analyzer software offers computational analysis of solutions using a large electrolyte thermodynamics network. The software offers temperature, pH, equilibrium, titration and pressure calculations among others and can compute viscosity, density, enthalpy and compositions of the solution. The Stream Analyzer provides rapid calculations based on experimental and theoretical results that allows researchers to calculate properties of solutions given a few measurements or to hypothetically test parameters before consuming time and resources in the laboratory. Due to the novel nature of calcium phosphosilicate nanoparticles, OLI's thermodynamic database does not contain any information regarding its properties. Fortunately, the database contains extensive data on the substituent ions calcium, phosphate, and silicate in aqueous systems and the model system hydroxyapatite, as well as all other known calcium phosphates. Experimental results from calcium ion selective electrode measurements and inductively coupled plasma – atomic emission spectroscopy were used to determine the input parameters to simulate the chemical environment of calcium phosphosilicate nanoparticles for the development of a provisional solubility product. Once a quantitative solubility is determined, the novel materials can be incorporated into OLI Systems thermodynamic databases and the thermodynamic framework used to simulate the behavior of CPSNPs in a variety of conditions.

5.1 Introduction to OLI Systems and Electrolyte Thermodynamics Simulations

OLI Systems offers a large and predictive thermodynamic framework and thus is highly desirable for predicting the solubility of a novel material such as calcium phosphosilicate once experimental parameters are input. The OLI thermodynamic framework can calculate physical and chemical properties of multi-phase aqueous systems through the Aqueous framework, which will be the database used to calculate a provisional k_{sp} in this study. Additionally, OLI employs a Mixed-Solvent Electrolyte framework for aqueous-organic systems, which is relevant to determining solubility in 70:30 ethanol:water systems once quantitatively established, as well as data relevant to oil field chemistry, corrosion, and process modeling, which were not explored in this project.

OLI contains an extensive public database permitting users to compute chemical and phase behaviors of steady-state or dynamic processes in single-point or multi-point iterations for 80 inorganic elements and their ionic species and over 8000 organic compounds.²⁶ Perhaps the largest benefit of OLI Systems for this project is the ability to create and maintain a private database, which allows calculations across virtually any conditions for the novel calcium phosphosilicate material by simply coding for the provisional k_{sp} determined and inputting the measured ionic stoichiometries. By creating this material in a database, complex phase analysis can be performed to predict how the nanoparticles will behave in aqueous and physiological solutions, which will grant us an understanding of their chemistry and allow tailoring to the specific needs of a cancer delivery vehicle.

5.2 OLI Systems Parameters for the Solubility of CPSNPs

Measured calcium activities combined with stoichiometric elemental ratios from inductively coupled plasma – atomic emission spectroscopy (ICP-AES) were integrated into the OLI Studio Stream Analyzer v9.5 to determine the theoretical aqueous composition where traditional experimental analysis falls short. Determined calcium activities were binned to the nearest tenth of a pH unit for each sample analyzed and the mean activity with 95% confidence interval was calculated. In OLI Studio Stream Analyzer, isothermal calculations were performed at the set binned pH value. The species parameters for 1 volume% PBS (per Corning Cellgro Buffered Saline Solutions Formulations) were input as stream inflows and adjusted to be the amount present in 1 L to simplify calculations. The average calcium activity for a given pH value was converted to the amount of calcium in moles and input as CaCl_2 , using the chloride ion to balance the charge and minimize competing reactions that would accompany other anions. Silicate was input as the formulation species used, Na_2SiO_3 , and the input in moles was determined by the molar ratio compared to calcium from ICP-AES analysis. All solid species were excluded from the chemistry model, preventing hydroxyapatite and other calcium phosphates from interfering with calculations and skewing results. The aqueous $[\text{Ca}^{2+}]$, $[\text{PO}_4^{3-}]$, $[\text{HPO}_4^{2-}]$, $[\text{H}_2\text{PO}_4^-]$, $[\text{SiO}_2]$, and $[\text{OH}^-]$ calculated for each binned pH and sample were then used to calculate a provisional solubility product for each sample using the measured Ca, P, and Si elemental ratios from ICP-AES. An example of the input parameters for a generic sample at pH 8.7 is shown below in Figure 10. Because all samples for calcium ion activity were measured in 1 volume % PBS, the phosphate salt inputs remained constant across all calculations and only the amount of CaCl_2 , Na_2SiO_3 , and pH changed depending on the specific sample.

Variable	Value
Stream Parameters	
Stream Amount (mol)	55.5084
Temperature (°C)	25.0000
Pressure (atm)	1.00000
Calculation Parameters	
Target pH	8.70000
Use Single Titrant	No
pH Acid Titrant	HCl
pH Base Titrant	NaOH
Inflows (mol)	
H2O	55.5082
KH2PO4	1.06000e-6
NaCl	1.54000e-4
Na2HPO4	5.60000e-6
CaCl2	1.20000e-5
Na2SiO3	2.21000e-6
HCl	0.0
NaOH	0.0

Figure 10. Sample OLI Systems stream input parameters for generic pH 8.7 CPSNPs. The $[Ca^{2+}]$, $[PO_4^{3-}]$, $[HPO_4^{2-}]$, $[H_2PO_4^-]$, $[SiO_2]$, and $[OH^-]$ obtained from the speciation results were used to develop a provisional k_{sp} for each sample of CPSNPs.

The input parameters to determine ionic concentrations in simulated CPSNP suspensions were: Temperature = 25.0 °C, Pressure = 1 atm, H₂O = 1000 g, KH₂PO₄ = 0.00144 g, NaCl = 0.09 g, and Na₂HPO₄ = 0.00795 g. The mass of CaCl₂, mass of Na₂SiO₃, and the specific pH value varied depending on the calcium activity measured, pH observed, and elemental ratios from ICP-AES and are compiled in Appendix C. Ionic species outputs from OLI Studio Stream Analyzer can also be found in Appendix C, along with the calculated aggregate solubility products.

5.3 Experimentally Determined Solubility of CPSNPs

The determined OLI Systems stream output species from the previous section were combined with the elemental ratios from ICP-AES analysis to determine a provisional k_{sp} for each binned pH by multiplying the concentrations of each ion raised to the power of their stoichiometric coefficients. The provisional k_{sp} for each sample was then determined by statistically weighing the

results from each pH to create an average pk_{sp} for each of the three samples. The calculations, concentrations used, charge balance, and solubility statistics for each binned pH and sample can be found in Appendix C. The chemical formulas, molecular weights, and statistically weighted k_{sp} for each sample were input into OLI's ESP 9.6 program to create three new species, JMM245, JMM263, and JMM264 in the chemical database. Back in OLI Studio Stream Analyzer, these databases were imported, and titrations were simulated for each species. Simulated titrations provided quantitative predictions about how each CPSNP species performs under various conditions. Titrations were computed under standard aqueous conditions and under physiological electrolyte conditions.

Table 11. Provisional solubility products and charge-balanced chemical formulas for each of the three 1X cit-Ghost CPSNP samples analyzed by ICP-AES and calcium ISE. These chemical formulas and solubility data were input into the OLI Systems ESP 9.6 program to create three new species, JMM245, JMM263 and JMM 264, which allowed for their titration and subsequent chemical analysis in OLI Systems.

Sample	Charge-Balanced Formula	Model Ca:P System	$\text{pk}_{\text{sp}} \pm 95\% \text{ CI}$
JMM 2-45	$\text{CaNa}_{0.7}(\text{H}_2\text{PO}_4)_{2.7}(\text{SiO}_2)_{2.87}$	Monocalcium phosphate	35.3 ± 0.2
JMM 2-63	$\text{Ca}_8\text{Na}_{0.43}(\text{PO}_4)_{4.11}(\text{HPO}_4)_{2.05}(\text{SiO}_2)_{8.27}$	Octacalcium phosphate	120.2 ± 0.3
JMM 2-64	$\text{Ca}(\text{HPO}_4)_{0.92}(\text{SiO}_2)_{0.97}(\text{OH})_{0.16}$	Dicalcium phosphate	14.3 ± 0.0

5.4 Thermodynamic Analysis of CPSNP Solubility in OLI Systems

With the thermodynamic parameters for each of the observed CPSNP species firmly established and input into the OLI ESP 9.6 program, the databanks were imported to OLI Studio Stream Analyzer and each species was analyzed in the same manner as other well-established

inorganic species are analyzed, such as brushite, hydroxyapatite, calcium chloride, etc. Because each calcium phosphosilicate species was modeled after a common calcium phosphate with similar Ca:P ratio, CPSNP species were first compared to the established species. Monocalcium phosphate monohydrate was compared to JMM245, octacalcium phosphate pentahydrate was compared to JMM263, and dicalcium phosphate dihydrate was compared to JMM264. Because the CPSNP reverse-micelle synthesis occurs in an aqueous environment, it was assumed the calcium phosphosilicate species would exist in a hydrated state. With no metric to measure the hydration state of the calcium phosphosilicates, the coordinated water molecules were excluded from their thermodynamic parameters, but this provided the rationale for comparing them to the hydrated states of the known calcium phosphates.

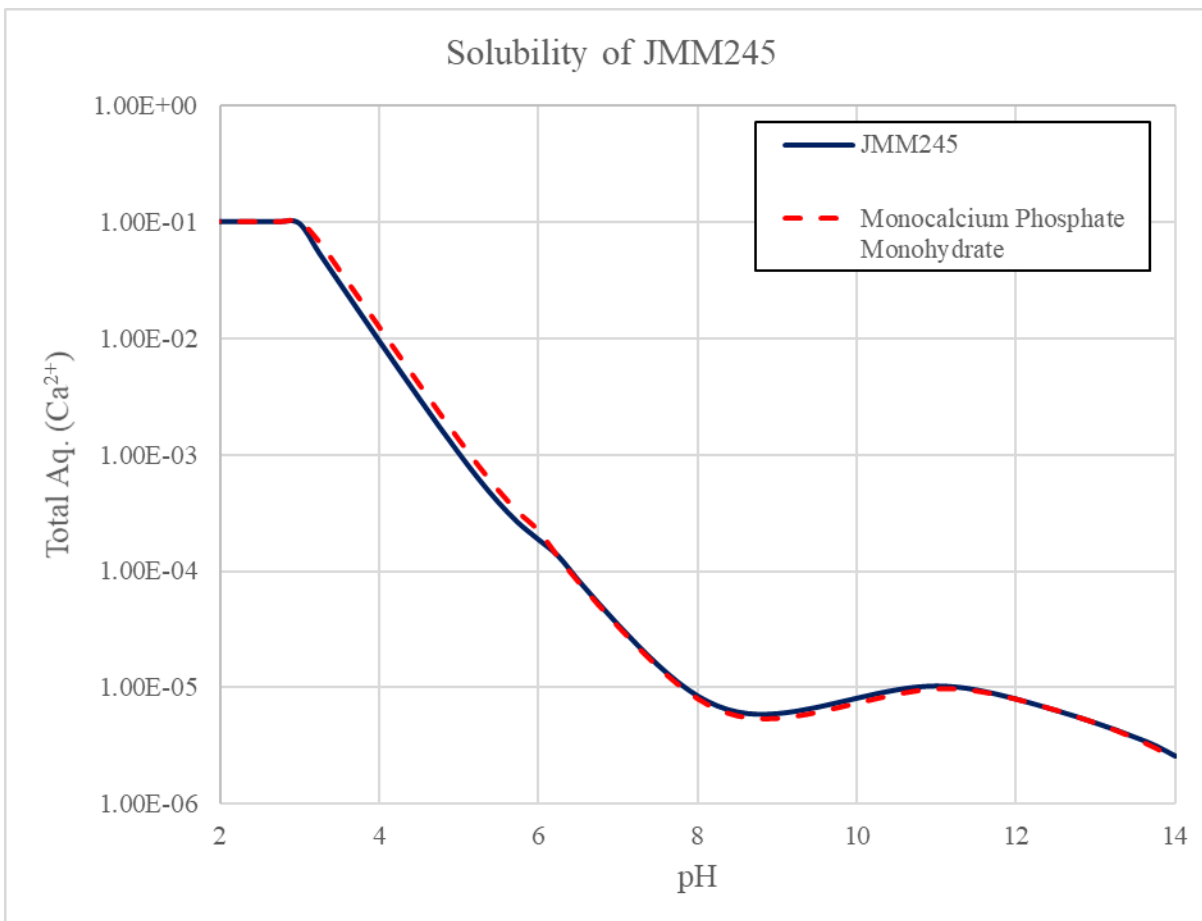


Figure 11. Comparison of the solubility of the calcium phosphosilicate species JMM245 and monocalcium phosphate monohydrate ($\text{Ca}(\text{H}_2\text{PO}_4)_2 \cdot \text{H}_2\text{O}$) using equimolar amounts. Total Aq. (Ca^{2+}) is the sum of all aqueous calcium species and is a more representative proxy of solubility than the concentration of calcium in solution, $[\text{Ca}^{2+}]$, because it accounts for intermediate species. The solubility of JMM245 closely mirrors the solubility of monocalcium phosphate monohydrate, confirming the hypothesis that JMM245 is a monocalcium phosphate-like species.

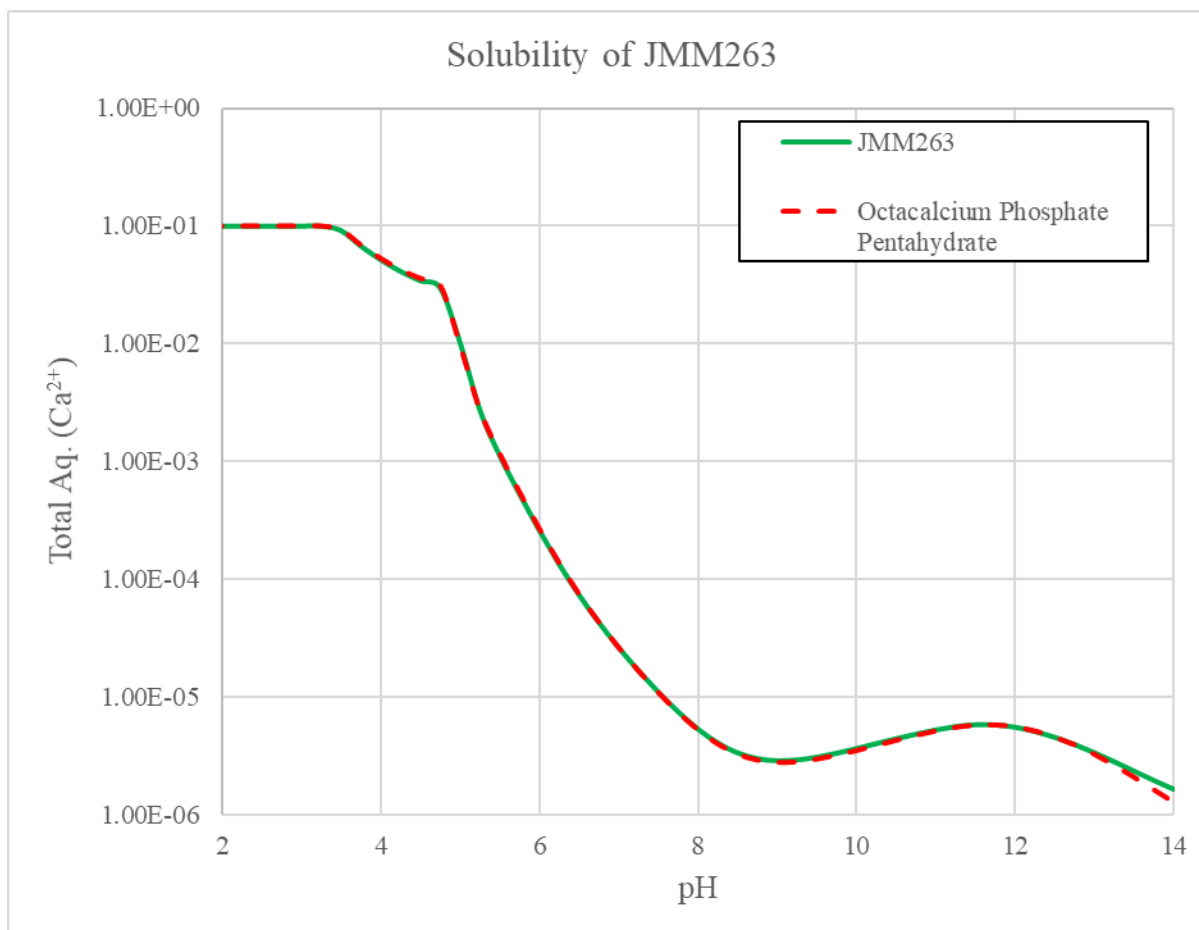


Figure 12. Comparison of the solubility of the calcium phosphosilicate species JMM263 and octacalcium phosphate pentahydrate ($\text{Ca}_8(\text{HPO}_4)_2(\text{PO}_4)_4 \cdot 5\text{H}_2\text{O}$) using equimolar amounts. Total Aq. (Ca^{2+}) is the sum of all aqueous calcium species and is a more representative proxy of solubility than the concentration of calcium in solution, $[\text{Ca}^{2+}]$, because it accounts for intermediate species. The solubility of JMM263 agrees well with the solubility of octacalcium phosphate pentahydrate, again confirming the hypothesis that JMM263 behaves as an octacalcium phosphate-like species.

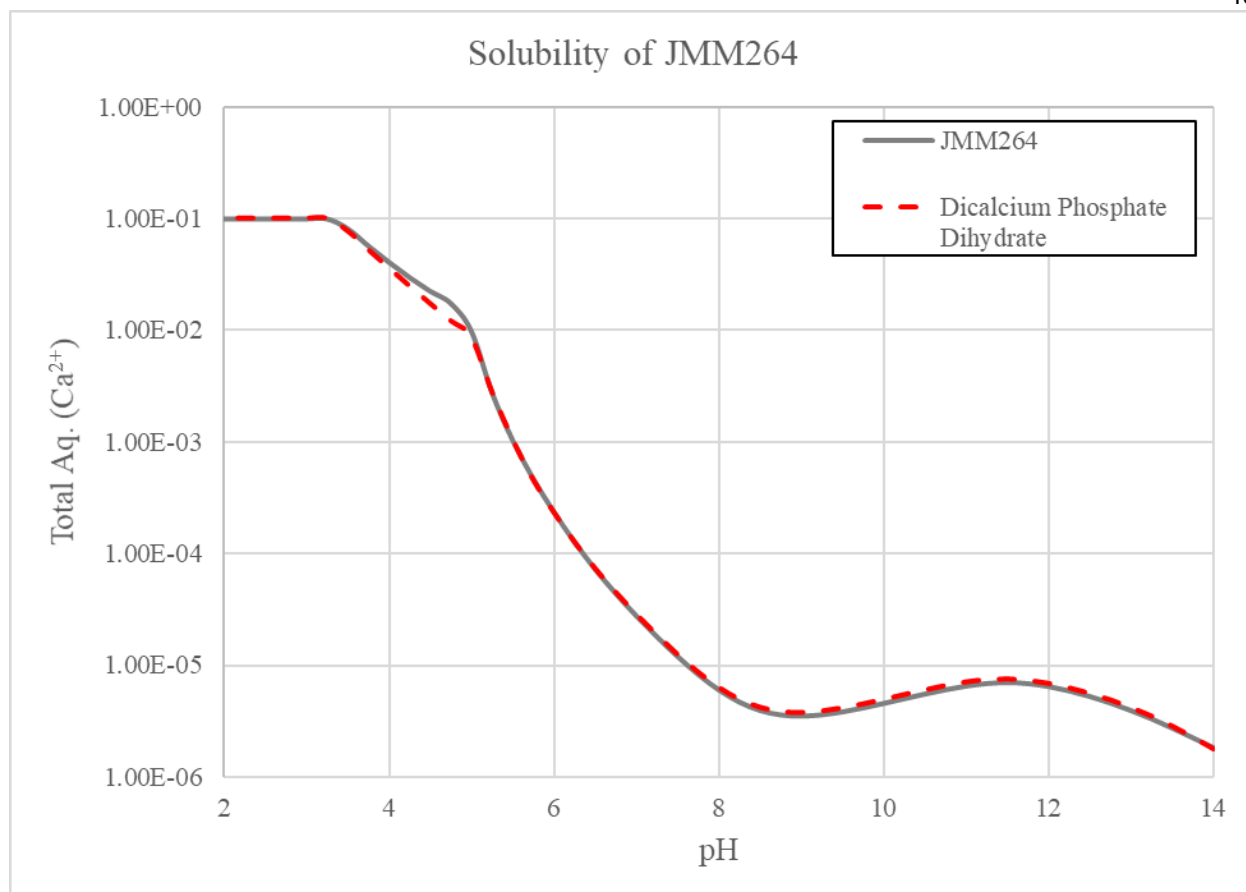


Figure 13. Comparison of the solubility of the calcium phosphosilicate species JMM264 and dicalcium phosphate dihydrate ($\text{CaHPO}_4 \cdot 2\text{H}_2\text{O}$) using equimolar amounts. Total Aq. (Ca^{2+}) is the sum of all aqueous calcium species and is a more representative proxy of solubility than the concentration of calcium in solution, $[\text{Ca}^{2+}]$, because it accounts for intermediate species. The solubility of JMM264 matches well with the solubility of dicalcium phosphate dihydrate, confirming the hypothesis that JMM264 behaves as a dicalcium phosphate-like species.

Figures 11-13 above compare the calcium phosphosilicate species to its analogous calcium phosphate. The striking similarities in each of the figures among the two solubility curves in each graph have important implications. First, these results confirm the hypothesis that the calcium phosphosilicate nanoparticles partition into a pseudo-calcium phosphate phase comparable by Ca:P ratio. Comparing these results to Figure 1, this hypothesis agrees with the fact that most calcium phosphates, other than hydroxyapatite, have nearly identical solubility, especially in the

pH 6-8 range. This also agrees with the calcium ion selective electrode experimental results in Figure 8. Despite having different Ca:P ratios and elemental concentrations determined by ICP-AES, the three observed CPSNP samples have very similar solubility. Another explanation for the congruency among the amorphous nanoparticle results and the crystalline predictions is the hypothesis that calcium phosphates undergo a solution-mediated solid-solid phase transformation through a hydroxyapatite phase. Boskey and Posner reported the formation of microcrystalline hydroxyapatite in the phase transition of amorphous calcium phosphate.²⁷ It is unclear how these effects translate when silica is incorporated into the amorphous matrix and further studies will be required to resolve this relationship in calcium phosphosilicate nanoparticles.

These similarities among calcium phosphosilicates and calcium phosphates also reinforce the Adair group's longstanding hypothesis that although amorphous calcium phosphates are more soluble than crystalline forms, the addition of silica into the matrix suppresses dissolution. By incorporating silica into the nanocomposite, the CPSNPs resemble an amorphous form of monocalcium phosphate, octacalcium phosphate, or dicalcium phosphate. With three different calcium phosphate-based phases observed in the three CPSNP samples and two more observed in the earlier ICP-AES and EELS results of Figure 9, it is possible that CPSNPs partition into even more calcium phosphate phases during synthesis, most notably hydroxyapatite. The pseudo-hydroxyapatite phase of JMM 2-17 in Figure 9 is most notable because it mimics the synthetic precursor inputs, hinting at a near 100% incorporation of the constituent ions. This was not the case for the other observed phases.

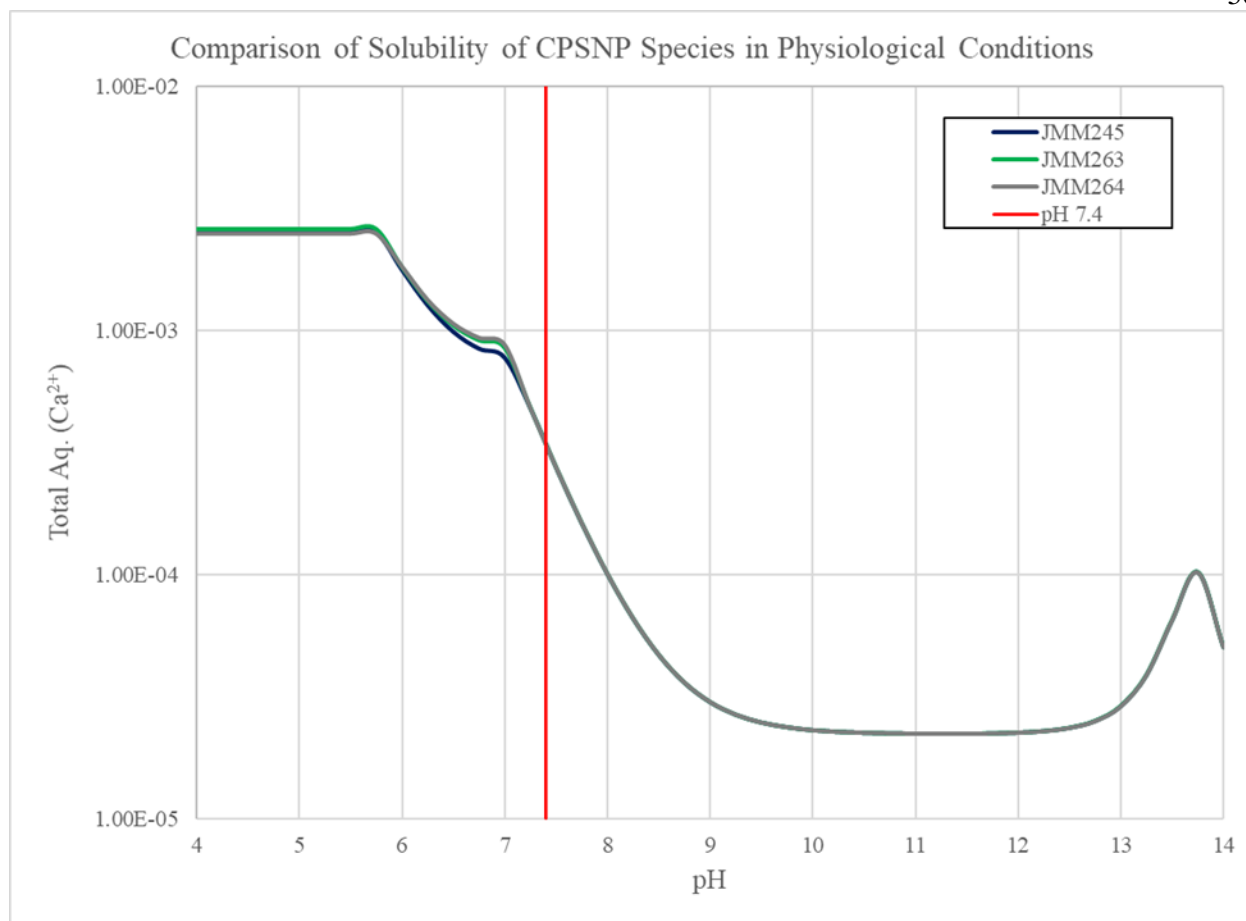


Figure 14. Solubility of calcium phosphosilicate species JMM245, JMM263, and JMM 264 in physiological conditions of human plasma. Human plasma has the composition Na^+ 142, K^+ 5, Mg^{2+} 1.5, Ca^{2+} 2.5, HPO_4^{2-} 1, Cl^- 103, HCO_3^- 27, and SO_4^{2-} 0.5 mmol/L. At pH 7.4 plasma conditions, all calcium phosphosilicate species are insoluble. Upon reaching the pH 5 environment of the late endosome within a cell, the CPSNPs are completely dissolved, thus effectively releasing the encapsulated molecule.

Figure 14 shows the solubility of the three calcium phosphosilicates under physiological conditions. Notably, these physiological conditions simulate human plasma, where CPSNPs must remain stable and insoluble until they reach their targeted cell. Human plasma is reported to have the following electrolytes: $\text{Na}^+ = 142$ mmol/L, $\text{K}^+ = 5$ mmol/L, $\text{Mg}^{2+} = 1.5$ mmol/L, $\text{Ca}^{2+} = 2.5$ mmol/L, $\text{HPO}_4^{2-} = 1$ mmol/L, $\text{Cl}^- = 103$ mmol/L, $\text{HCO}_3^- = 27$ mmol/L, and $\text{SO}_4^{2-} = 0.5$ mmol/L.²⁸ At pH 7.4, the CPSNPs remain sparingly soluble. As the pH value approaches pH 5 from the physiological 7.4, the nanoparticles completely dissolve, permitting the release of the

encapsulated drug. These results quantitatively confirm the previous *in vivo* results, which showed the particles remain intact in the bloodstream and selectively dissolve in the late endo-lysosome of a cancerous cell. It is also important to note that the CPSNPs studied in this experiment are treated with citrate to prevent agglomeration. The chelation of citrate may affect the solubility at the surface of the calcium phosphosilicate nanoparticles. These results are valid for the interior of the particles, which are not chelated by citrate.

The results reported in this study have implications critical to advancing our understanding of calcium phosphosilicate nanoparticles to tailor the solubility to fit a pre-determined need and understand the release mechanism. Physiological fluids are complex solutions of electrolytes, proteins, and other biomolecules that all influence the chemistry of each other. In designing a nanoparticle platform for targeted drug delivery, flexibility in the solubility is important for creating a delivery system for a wide variety of needs. Calcium phosphosilicate nanoparticles have been studied extensively for their ability to selectively dissolve in low pH environments within tumors. With a more thorough understanding of the chemistry, it is now possible to expand the studies of CPSNPs on treating cancers and begin to investigate the potential of CPSNPs in other aspect of medicine, such as delivering antibiotics, anti-inflammatories, and antiviral medication, among others, to open the possibilities of treating more human conditions and advancing medicine.

Appendix A

Development of Calcium Ion Selective Electrode Protocol

The development of a suitable protocol for calcium ion activity determination by means of calcium ion selective electrode was an iterative process, modified over time to achieve the most reproducible and consistent results across the suspected calcium activity range. An ion selective electrode was initially chosen for its non-destructive means of measuring the ionic activity of $\text{Ca}^{2+}(\text{aq})$ in a sample. The goal was that once a robust protocol was developed, all synthetic samples could be easily characterized as a method of quality control.

A handheld calcium ion selective electrode was initially chosen as a compact way to measure the calcium but was found to be not capable of measuring the low levels of calcium in the CPSNP samples. To further complicate that, it was desired to measure CPSNP samples in a diluted phosphate-buffered saline, which suppresses calcium dissolution via the common ion effect but also will simplify calculations by adding a known quantity of phosphate that is significantly larger than the phosphate species dissolved from the nanoparticles. By doing this, calculations would be simplified by neglecting the negligible amount of phosphate released from the nanoparticles and only using the known amount added from the PBS. On the initial handheld meter, CPSNP samples were tested in solutions of PBS ranging from undiluted (10 mM phosphates) to 0.01% PBS by volume. With calcium ion activity measurements still below the range of the instrument, it became necessary to pursue a probe with a lower limit of detection. At this point, the Cole-Parmer Calcium Ion Selective Electrode, with a lower-limit of detection of 0.2 ppm Ca^{2+} , became the primary instrument for calcium ion activity analysis.

With a probe now selected, it became necessary to develop an accurate and efficient calibration protocol to measure CPSNP samples. The present protocol is based on the low-level calcium determination in the provided instruction manual using a pH/mV meter. To maximize the representativeness of the calibration curve solutions relative to the samples measured, it was necessary to calibrate the probe in solutions of the same ionic strength as the samples. Because the samples would be measured in PBS diluted to 1% by volume, the calibration was performed in the same 1 volume % PBS solution. As the activity coefficient and therefore the activity of an ion varies with the ionic strength of the solution, it was necessary to calibrate the probe in a solution of identical ionic strength.

Appendix B

Development of CPSNP Drying Protocol: The Hydroxyapatite Story

With an adequate calcium ion activity measurement protocol now in place, the focus shifted to iterations to statistically determine and validate a calcium activity for CPSNPs. To do this, initial iterations were performed side-by-side with measurements of saturated hydroxyapatite solutions in the same diluted PBS buffer (1 vol%). Albeit slightly lower than the theoretical values of hydroxyapatite in 1 volume % PBS, the calcium activities for hydroxyapatite samples followed the theoretical solubility trend produced using OLI Systems consistently and proved to be an efficacious method to measure the calcium activity of a sample in solution. When the hydroxyapatite calcium activities were compared to the calcium activities of CPSNP samples under the same conditions, it became apparent that the solubility of CPSNPs mimicked the solubility of hydroxyapatite and followed the same approximate curve of measured values. These results, shown below in Figure 15, sharply contrasted with the hypothesis that the amorphous nature of the particles would yield a material more soluble than hydroxyapatite. This raised the question: does hydroxyapatite exist, in any form, in the nanoparticle formulations?

Attention was immediately turned to the traditional drying process which involved drying the 70:30 ethanol:water nanoparticle suspensions under a flow of argon. In this process, once nearly all of the ethanol (and some of the water due to azeotropic effect at 95:5 ethanol:water) has evaporated, the remaining solution will be nearly 100% water with CPSNPs in suspension. At this point, it is possible and probable that the nanoparticles partially or wholly dissolve from their

metastable state, which is expected in the aqueous environment, and recrystallize as hydroxyapatite via a solution-mediated phase transformation. This may take the form of whole particle dissolution, but possibly only involves semi-crystallization of the external layer of the calcium phosphosilicate nanoparticles.

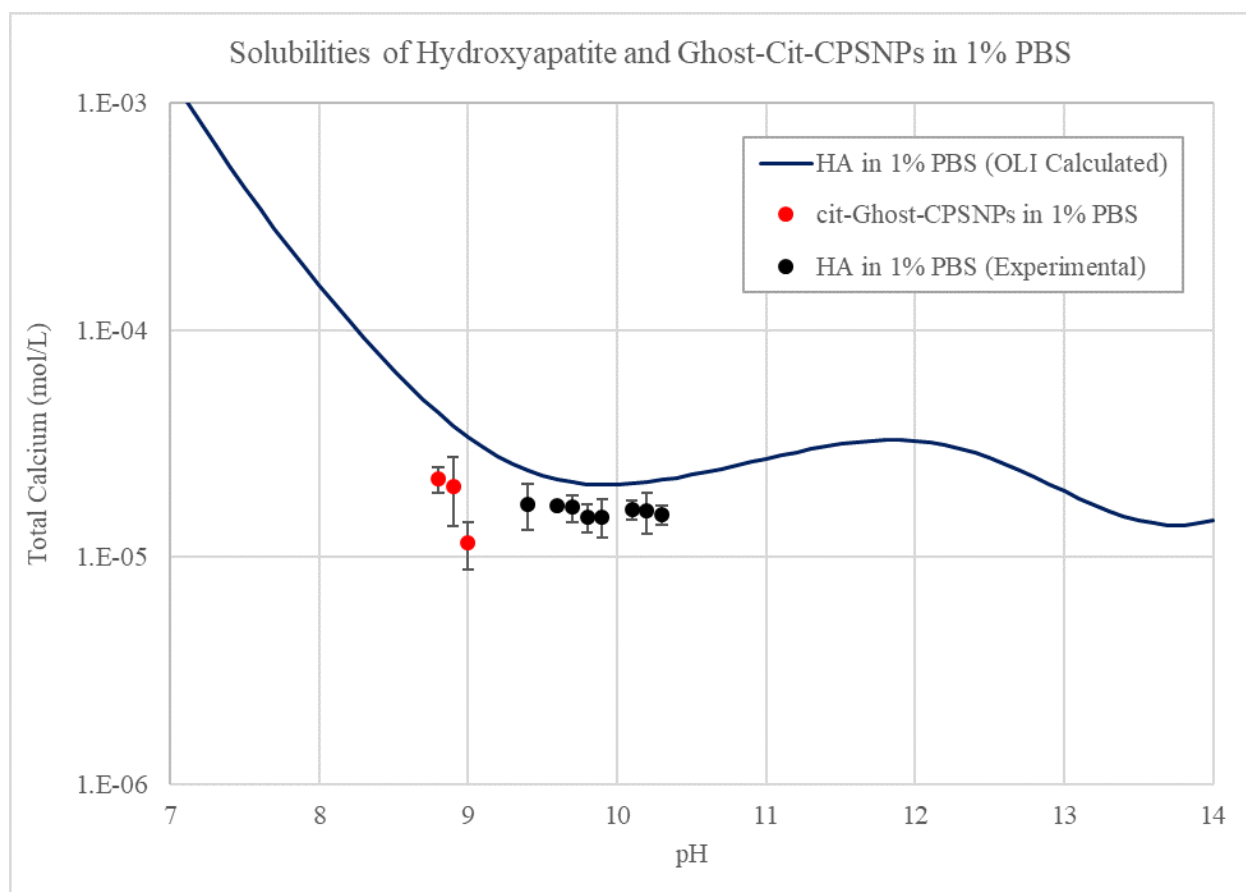


Figure 15. Comparison of theoretical calcium activity of hydroxyapatite with experimental calcium activities of Ghost-CPSNP and hydroxyapatite samples, all in 1% PBS. The similarities in activities of cit-Ghost-CPSNP samples and hydroxyapatite samples prompted the hypothesis that recrystallization was occurring during the drying procedure, resulting in hydroxyapatite-coated particles and hydroxyapatite-like results. This hypothesis prompted the development of the current drying protocol, which involves the addition of PBS before drying to prevent dissolution.

To correct for this, a new drying protocol was developed. Because nanoparticles would be later suspended in a PBS solution, it was logical to add a pre-defined volume of PBS prior to drying so that once dried to a solid, only a specified volume of pure water needed to be added to the

sample to achieve the desired concentration of PBS. By adding PBS, the common ion effect of the phosphate suppressed dissolution of the nanoparticles and retain the amorphous features and characteristics in the latter stages of drying.

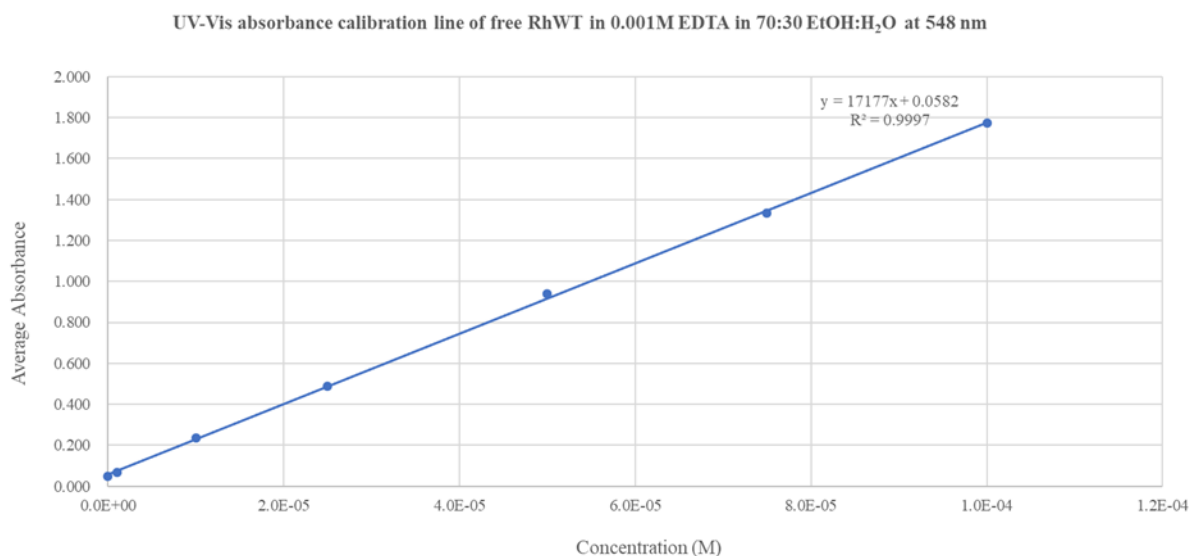


Figure 17. UV-Vis calibration curve used to determine the concentration of RhWT in a cit-RhWT CPSNP sample as a proxy for encapsulation efficiency.

Table 12. Specifications of Phosphate Buffered Saline (PBS) from Corning Cellgro. PBS was used to suppress dissolution in calcium ion activity measurements and the species were input into OLI Systems for relevant calculations.

Catalog Number	21-040
Description	Liquid, 1x
Units	g/L
KH ₂ PO ₄	0.144
NaCl	9.00
Na ₂ HPO ₄	0.795

Table 13. Relevant inputs and outputs from OLI Studio's Stream Analyzer used to compile a provisional solubility product for each CPSNP sample. The elemental ratios were obtained from ICP-AES analysis and charge-balanced with Na^+ , the dominant secondary cation in the synthesis or OH^- , the standard charge balancing anion of calcium phosphates. Only the input $[\text{Ca}^{2+}]$ and amount of silicate were varied for each pH and synthesis. The calcium added was determined by calcium ion selective electrode and the silicate added was determined via ICP ratio relative to calcium. For calculations, all solid species were excluded to prevent competing reactions.

	JMM 2-45		JMM 2-63		JMM 2-64	
pH	8.7	8.9	8.7	8.8	8.7	9.0
(Ca2+) ppm	0.575	0.481	0.453	0.510	0.483	0.532
(Ca2+) M	1.44E-05	1.20E-05	1.13E-05	1.28E-05	1.21E-05	1.33E-05
Ca2+ Activity Coeff (γ)	0.828	0.828	0.828	0.828	0.828	0.828
[Ca2+] M	1.74E-05	1.45E-05	1.37E-05	1.54E-05	1.46E-05	1.61E-05
[Ca2+] g/L of CaCl2	1.93E-03	1.61E-03	1.52E-03	1.71E-03	1.62E-03	1.78E-03
Silicate Input g/L	6.07E-03	5.08E-03	1.73E-03	1.94E-03	1.72E-03	1.90E-03
OLI SYSTEMS OUTPUTS						
[Ca2+] M	1.65E-05	1.34E-05	1.30E-05	1.44E-05	1.38E-05	1.46E-05
Ca2+ Coefficient	1.00	1.00	8.00	8.00	1.00	1.00
[PO4 3-] M	1.94E-08	3.10E-08	1.94E-08	2.45E-08	1.94E-08	3.88E-08
PO4 Coefficient	0	0	4.11	4.11	0	0
[HPO4] M	6.39E-05	6.43E-05	6.41E-05	6.42E-05	6.40E-05	6.42E-05
HPO4 Coefficient	0	0	2.05	2.05	0.92	0.92
[H2PO4] M	1.76E-06	1.12E-06	1.77E-06	1.41E-06	1.77E-06	8.91E-07
H2PO4 Coefficient	2.70	2.70	0	0	0	0
[SiO2] M	4.56E-05	3.64E-05	1.30E-05	1.43E-05	1.29E-05	1.32E-05
SiO2 Coefficient	2.87	2.87	8.27	8.27	0.97	0.97
[OH-]	5.34E-06	8.46E-06	5.33E-06	6.71E-06	5.33E-06	1.06E-05
OH- Coefficient	0	0	0	0	0.16	0.16
[Na+]	1.75E-03	1.73E-03	1.68E-03	1.68E-03	1.68E-03	1.68E-03
Na+ Coefficient	0.7	0.7	0.43	0.43	0	0
CALCULATIONS						
Charge	0	0	0	0	0	0
Charge Balanced ksp	1.96E-35	2.45E-36	1.02E-121	1.36E-120	4.97E-15	6.01E-15
Charge Balanced pksp	34.7	35.6	121.0	119.9	14.3	14.2
Weighted Average pksp	35.3		120.2		14.3	
Std. Dev.	0.4		0.5		0.0	
95% Confid. Inter.	0.2		0.3		0.0	
Molecular Weight (g/mol)	490.479		1414.497		186.822	

BIBLIOGRAPHY

- (1) Altinoglu, E.; Adair, J. H. Calcium Phosphate Nanocomposite Particles: A Safer and More Effective Alternative to Conventional Therapy? *Future Oncol.* **2009**, *5*, 279–281.
- (2) Adair, J. H.; Parette, M. P. Nanoparticulate Alternatives for Drug Delivery - ACS Nano. **2010**, *4* (9), 4967–4970.
- (3) Wilczynski, Z. R. Synthesis and Optimized Laundering of Calcium Phosphosilicate Nanoparticles for Imaging and Treatment of Metastatic Breast Cancer, The Pennsylvania State University, 2017.
- (4) Sahoo, S. K.; Labhasetwar, V. Nanotech Approaches to Drug Delivery and Imaging. *Drug Discov. Today* **2003**, *8* (24), 1112–1120.
- (5) Yih, T. C.; Al-Fandi, M. Engineered Nanoparticles as Precise Drug Delivery Systems. *J. Cell. Biochem.* **2006**, *97* (6), 1184–1190.
- (6) Nakamura, Y.; Mochida, A.; Choyke, P. L.; Kobayashi, H. Nanodrug Delivery: Is the Enhanced Permeability and Retention Effect Sufficient for Curing Cancer? *Bioconjug. Chem.* **2016**, *27* (10), 2225–2238.
- (7) Li, P.; Ohtsuki, C.; Kokubo, T.; Nakanishi, K.; Soga, N.; Nakamura, T.; Yamamuro, T. Apatite Formation Induced by Silica Gel in a Simulated Body Fluid. *J. Am. Ceram. Soc.* **1992**, *75* (8), 2094–2097.
- (8) Chander, S.; Fuerstenau, D. W. Interfacial Properties and Equilibria in the Apatite-Aqueous Solution System. *J. Colloid Interface Sci.* **1979**, *70* (3), 506–516.
- (9) Tacelosky, D. M.; Creecy, A. E.; Shanmugavelandy, S. S.; Smith, J. P.; Claxton, D. F.; Adair, J. H.; Kester, M.; Barth, B. M. Calcium Phosphosilicate Nanoparticles for Imaging and Photodynamic Therapy of Cancer. *Discov Med* **2012**, *13* (71), 275–285.
- (10) Tabaković, A.; Kester, M.; Adair, J. H. Calcium Phosphate-Based Composite Nanoparticles in

- Bioimaging and Therapeutic Delivery Applications. *Wiley Interdiscip. Rev. Nanomedicine Nanobiotechnology* **2012**, 4 (1), 96–112.
- (11) Barth, B. M.; Sharma, R.; Altinoğlu, E. I.; Morgan, T. T.; Shanmugavelandy, S. S.; Kaiser, J. M.; McGovern, C.; Matters, G. L.; Smith, J. P.; Kester, M.; et al. Bioconjugation of Calcium Phosphosilicate Composite Nanoparticles for Selective Targeting of Human Breast and Pancreatic Cancers In Vivo. *ACS Nano* **2010**, 4 (3), 1279–1287.
- (12) Chander, S.; Fuerstenau, D. W. On the Dissolution and Interfacial Properties of Hydroxyapatite. *Colloids and Surfaces* **1982**, 4 (2), 101–120.
- (13) Mellman, I.; Fuchs, R.; Helenius, A. Acidification of the Endocytic and Exocytic Pathways. *N. Engl. J. Med.* **1960**, 262 (1), 45–45.
- (14) Gerweck, L. E.; Seetharaman, K. Cellular PH Gradient in Tumor versus Normal Tissue: Potential Exploitation for the Treatment of Cancer. *Cancer Res.* **1996**, 56 (6), 1194–1198.
- (15) Eanes, E. D.; Termine, J. D.; Nysten, M. U. An Electron Microscopic Study of the Formation of Amorphous Calcium Phosphate and Its Transformation to Crystalline Apatite. *Calcif. Tissue Res.* **1973**, 12 (1), 143–158.
- (16) Dorozhkin, S. V. Calcium Orthophosphates. *J Mater Sci.* **2007**, 1061–1095.
- (17) Moreno, E. C.; Gregory, T. M.; Brown, W. E. Preparation and Solubility of Hydroxyapatite. *J. Res. National Bureau of Standards*, **1968**, 72 (6), 773–782.
- (18) Clark, J. Solubility Criteria for the Existence of Hydroxyapatite. *Can. J. Chem.* **1955**, 1696–1700.
- (19) Muddana, H. S.; Morgan, T. T.; Adair, J. H.; Butler, P. J.; Pennsylv, V. Photophysics of Cy3-Encapsulated Calcium Phosphate Nanoparticles. *Nano Lett.* **2009**, 1559–1566.
- (20) Altinoğlu, E. I. Indocyanine Green-Encapsulating Calcium Phosphosilicate Nanoparticles: Bifunctional Theranostic Vectors for Near Infrared Diagnostic Imaging and Photodynamic Therapy, The Pennsylvania State University, 2010.
- (21) Olesik, J. W. ICP-OES. **1974**, 633–644.

- (22) Sneddon, J.; Vincent, M. D. ICP-OES and ICP-MS for the Determination of Metals: Application to Oysters. *Anal. Lett.* **2008**, *41* (8), 1291–1303.
- (23) Olesik, J. W. Fundamental Research in ICP-OES and ICPMS. *Analytical Chem.* **1996**. 469-474.
- (24) Chow, L. C. Solubility of Calcium Phosphates. *Monogr. Oral Sci.* **2001**, 94-111.
- (25) Biomaterials, B.; Sheikh, Z.; Abdallah, M.; Hanafi, A. A. Mechanisms of in Vivo Degradation and Resorption of Calcium Phosphate Mechanisms of in Vivo Degradation and Resorption of Calcium Phosphate Based Biomaterials. *Materials*, **2015**, *8*, 7913–7925
- (26) OLI Systems Inc. A Guide to Using OLI Analyzer Studio. **2014**.
- (27) Conversion, S.; Boskey, A. L.; Posner, A. S. Conversion of Amorphous Calcium Phosphate to Microcrystalline Hydroxyapatite. **1973**, *77* (19), 2313–2317.
- (28) Grases, F. Supersaturation of Body Fluids, Plasma and Urine, with Respect to Biological Hydroxyapatite. **2011**, 429–436.

Academic Vita of Jared M. May

The Pennsylvania State University | Class of 2019

jaredmichaelmay@gmail.com

Education

The Pennsylvania State University, Schreyer Honors College, University Park, PA
Bachelor of Science in Chemistry, Biology Minor with Honors in Chemistry

Awards and Recognition

Dean's List: 7/7 semesters
President's Freshman Award: 4.0 first semester GPA
Schreyer Gateway Scholar 2017
James R. Freid Chemistry Scholarship
Elizabeth and JP Smith Memorial Scholarship Recipient 2017
Union League of Philadelphia Scholarship Recipient 2015

Research Experience

Penn State, Department of Materials Science and Engineering, University Park, PA Fall 2017 – Spring 2019
Undergraduate Researcher

- Synthesized calcium phosphosilicate nanoparticles (CPSNPs) for chemotherapeutic drug encapsulation under Dr. James Adair
- Characterized nanoparticles using zeta potential, surface tension assays, ICP-AES, and ion selective electrodes
- Developed solubility product for the amorphous material using experimental results and thermodynamic parameters
- Developed assay to measure cytotoxic residual reagents used in bioconjugation
- Coded for new material in OLI Systems to generate pH-dependent solubility data
- Composed Honors Thesis: Determination of the Solubility of Calcium Phosphosilicate Nanoparticles for Targeted Drug Delivery

Virginia Tech, Department of Chemistry, Blacksburg, VA Summer 2017
NSF-Funded Undergraduate Researcher

- Developed a novel metal-organic framework (MOF) under Dr. Amanda J. Morris
- Incorporated carboxyphenyl-corrole ligand into Zr-based MOF by parameter screening
- Characterized organic ligand and MOF using ¹H NMR, APCI-MS, UV-Vis, PXRD and fluorimetry

Southeast Regional Meeting of the American Chemical Society, Charlotte, NC November 7-11, 2017
Research Presenter

- Presented poster based on research conducted at Virginia Tech in Photochemistry symposium to experts in field

Extracurricular Activities

Penn State, Division of Student Affairs Campus Recreation, University Park, PA Fall 2016 – Spring 2018
Lifeguard

- Provided lifeguard services to Penn State Aquatic Facilities
- Certified in First Aid, CPR, AED, Oxygen Administration and Water Rescue through American Red Cross
- Enforced safety protocol at each pool

Penn State Dance Marathon, Penn State Fall 2016 – Spring 2019
Dancer Relations Committee Member, EMS Liaison THON 2017, Weekend Warrior THON 2018

- Supported dancers physically, mentally, and emotionally during the 46-hour dance marathon
- Educated committee members about dancer safety, health, and preparation
- Communicated between dancers and Emergency Medical Services staff

Special Events Committee Member, Family Carnival Liaison THON 2019

- Provided support to execute various events including the THON 5K and 100 Days Until THON Celebration
- Planned and operated the Family Carnival for over 100 families impacted by childhood cancer

Independent Dancer Couple, THON 2019

- Fundraised over \$12,100 benefitting the Four Diamonds at Penn State Children's Hospital
- Selected in lottery system based on funds raised to dance in the 46-hour marathon

Penn State Global Medical Brigades, Penn State Spring 2017
Student Volunteer

- Volunteered on a medical mission trip to Nicaragua in May 2017 to operate free local medical clinics
- Assisted in-country physicians with caring for over 600 patients
- Educated the public about safe and healthy practices and dug a trench to provide a community with access to clean water

Phi Eta Sigma National Honor Society, Penn State Fall 2015
Student Member